REPORT DOCUMENTATION PAGE

ᴏᴜᴜ

The public reporting burden for this collection of information is estimated to average 1 hour per response, including the time for reviewing instructions, searching existing data sources, gathering and maintaining the data needed, and completing and reviewing the collection of information. Send comments regarding this burden estimate or any other aspect of this collection of information, including suggestions for reducing the burden, to Department of Defense, Washington Headquarters Services, Directorate for Information Operations and Reports (0704-0188), 1215 Jefferson Davis Highway, Suite 1204, Arlington, VA 22202-4302. Respondents should be aware that notwithstanding any other provision of law, no person shall be subject to any penalty for failing to comply with a collection of information if it does not display a currently valid OMB control number.
PLEASE DO NOT RETURN YOUR FORM TO THE ABOVE ADDRESS.

1. REPORT DATE *(DD-MM-YYYY)*	2. REPORT TYPE		3. DATES COVERED *(From - To)*
	Final		1 Jan 2001 - 31 Dec 2003

4. TITLE AND SUBTITLE	5a. CONTRACT NUMBER
Plasma Field Telemetry For Hypersonic Flight	
	5b. GRANT NUMBER
	F49620-01-1-0155
	5c. PROGRAM ELEMENT NUMBER

6. AUTHOR(S)	5d. PROJECT NUMBER
Mark J. Lewis	
	5e. TASK NUMBER
	5f. WORK UNIT NUMBER

7. PERFORMING ORGANIZATION NAME(S) AND ADDRESS(ES)	8. PERFORMING ORGANIZATION REPORT NUMBER
Department of Aerospace Engineering University of Maryland College Park, MD 20742	

9. SPONSORING/MONITORING AGENCY NAME(S) AND ADDRESS(ES)	10. SPONSOR/MONITOR'S ACRONYM(S)
Air Force Office of Scientific Research 4015 Wilson Blvd Mail Room 713 Arlington, VA 22203	AFOSR
	11. SPONSOR/MONITOR'S REPORT NUMBER(S)

12. DISTRIBUTION/AVAILABILITY STATEMENT

Distribution Statement A. Approved for public release; distribution is unlimited.

13. SUPPLEMENTARY NOTES

14. ABSTRACT

Air Force interest in pursuing a solution to telemetry through a plasma sheath has been renewed recently since the resulting methodology may dictate some hypersonic vehicle design requirements. (Note that the United States Air Force began researching solutions to telemetry through reentry plasma layers in 1959.) The design of a hypersonic vehicle is a complex series of trade-offs between highly coupled systems, including, hut not limited to, propulsion, control, volumetric, payload, fuel, structural, aerodynamic, mission, and telemetry requirements. One promising solution for allowing telemetry through plasma layers is through aerodynamic shaping of the vehicle leading edge to generate the desired plasma properties further downstream. Shaping of this type could possibly' allow for telemetry at the tail of the vehicle with minimal signal attenuation. However, aerodynamic modification of a hypersonic vehicle after production would be more difficult and costly than redesigning the vehicle to account for the telemetry requirements in the beginning.

15. SUBJECT TERMS

16. SECURITY CLASSIFICATION OF:			17. LIMITATION OF ABSTRACT	18. NUMBER OF PAGES	19a. NAME OF RESPONSIBLE PERSON
a. REPORT	b. ABSTRACT	c. THIS PAGE			Mark J. Lewis
U	U	U	UU		19b. TELEPHONE NUMBER *(Include area code)*

Standard Form 298 (Rev. 8/98)
Prescribed by ANSI Std. Z39.18

PLASMA FIELD TELEMETRY FOR HYPERSONIC FLIGHT

Ryan P. Starkey, Wilson Santos, Daniel Hoult, and Mark J. Lewis (PI)
Department of Aerospace Engineering
University of Maryland
College Park, Maryland 20742

Technical Monitor:
Charles H. Jones
412 TW/ENTI
Edwards AFB, California 93524

Period of Performance:

Jan. 1, 2003 – Dec. 31, 2003

ABSTRACT

Since the beginning of spaceflight, the problems associated with communication blackout caused by the ionized reentry plasma sheath have been studied. Since telemetry blackout originally caused great concern for manned reentry vehicles, ballistic missiles, and atmospheric flight test vehicles, there have been many proposed approaches and associated tests to alleviate the problem. This Testing and Evaluation research program is intended to address methods of active flowfield modification that may allow for uninterrupted transmission through the plasma sheath. This is not the first time that telemetry issues for hypersonic flight have been investigated; some of the methods of interest here have been tested experimentally while others were postulated theoretically, but required advances in certain technologies. Most of the methods considered were envisioned during the earliest days of the United States space flight program, but are becoming more realizable as the technologies and computational methodologies involved mature. In the first portion of this activity, a search for material on this topic produced a substantial number of relevant sources. Overviews of a number of historical flight tests and more recent ground tests for communication blackout alleviation techniques are included. Since the degree of severity of the communication blackout problem is dependent on vehicle configuration, flight velocity, and angle of attack, no clear recommendation can be made as to the one method that will allow for uninterrupted transmission for all possible scenarios. Numerical methods for simulating telemetry issues are also under development, based on direct simulation methodologies. The non-ionized solutions of sharp leading edge flows have been pursued, as a prelude to charged-flow solutions.

TABLE OF CONTENTS

TABLE OF FIGURES

NOMENCLATURE

A = matrix function

$\overline{B}$ = time-harmonic magnetic field, T

B = magnetic field, T

c = phase velocity, m/s

C = function parameter

$\overline{E}$ = time-harmonic electric field, V/m

E = electric field phasor, V/m

f = frequency, Hz

$\overline{F}$ = force, N

H = magnetic field phasor, T

j = imaginary number, $\sqrt{-1}$

k = wave number, 1/m

LHCP = left hand circularly polarized

m = mass, kg

n = particle number density, $1/m^3$

q = electronic charge, C

RHCP = right hand circularly polarized

t = time, s

T&E = test and evaluation

v = velocity, m/s

X = displacement, m

$\hat{x}, \hat{y}, \hat{z}$ = unit vectors

α = attenuation constant, 1/m

β = phase constant, rad/m

ε = dielectric permittivity, F/m

θ = propagation angle, deg

γ = propagation constant, 1/m

ν = electron collision frequency, 1/s

ω = angular frequency, rad/s

Subscripts

0   = free stream

1-3   = function numbers

c   = cyclotron

e   = electron

elec   = electric

eff   = effective

i   = ion

mag   = magnetic

p   = plasma

r   = relative

x,y,z   = coordinate directions

Superscripts

′   = real part

″   = imaginary part

+   = RHCP wave

−   = LHCP wave

ij   = tensor notation

I. Background

From the dawn of time mankind has dreamed of flight, to soar like the birds and venture to the stars. The first successful flight of the Wright Flyer opened a new frontier of possibilities. In a few short seconds, the cumulative dreams of humanity had suddenly become reality and in those few seconds a Pandora's box of new challenges had been opened. Challenges such as instrumentation and navigation, as well as, advancing the theoretical basis of propulsion, structures, and aerodynamics. In the years since that 1903 flight, mankind has pushed the limits of technology to fly faster and higher, venture to the moon and back, and probe the reaches of the universe. Each of these goals were achieved through extensive testing and evaluation (T&E) of state-of-the-art vehicle prototypes. As each new step was completed, dreams became grander, design tolerances became smaller, and test vehicles became increasingly complex. Associated with these changes, there were also increased government regulation, extensive cost cutting, and fundamental differences in acceptance of risk. Nowhere have these later changes been more devastating than in the test and evaluation (T&E) community where the burden of program success rests on their shoulders.

The days of free spending and the learn-as-you-go attitude that began the X-Plane experimental flight test program in the 1940's are long gone. Although the program remains, these ideologies have been replaced by the extensive use of ground testing, minimization of flight testing, and the crippling government stance that virtually mandates program cancellation at the first sign of a setback. Of course, many of these regulations come with good intentions, such as promoting safety, preservation of life and the environment, and necessitating good science over gut instinct.

Unfortunately, these regulations also rule out many of the learning aspects of flight testing in favor of ground testing and computer simulation.

For the realm of hypersonics (characterized by velocities greater than five times the speed of sound), ground testing is only possible to a certain point after which flight testing becomes necessary. The T&E of an operational air-breathing, hypersonic cruise vehicle will be a challenge. One of the major challenges will be the difficulty of radio frequency telemetry through a plasma field. During certain hypersonic regimes, the plasma field generated around a vehicle can cause signal attenuation or complete communication blackout. Standard T&E procedures require real time telemetry monitoring at all times, primarily for flight safety reasons. Without real time monitoring it is extremely difficult to make quick decisions on when to abort a flight. This safety issue becomes significant if the vehicle is capable of sustained hypersonic flight. (Note that Mach 10 flight allows travel to anywhere in the world in about an hour and a half; a strong military reason for developing a vehicle capable of such velocities.) A secondary reason for desiring the ability of real time telemetry is for catastrophe analysis. Data collected milliseconds prior to a catastrophe could be critical in determining the cause, especially at hypersonic velocities (greater than about 1.5 km/s). In this case, real time data telemetry could be absolutely critical since the velocities and altitudes involved imply that it is unlikely that onboard recorders would survive a crash (or found if they do survive). A tertiary reason for real time monitoring is flight point validation. This is mostly a cost issue, but during normal envelope expansion, it is faster and cheaper to be able to verify a test point during flight and proceed to the next test point without having to land and takeoff in between.

Telemetry through plasma layers becomes essential when acknowledging the fact that most air-breathing hypersonic vehicle concepts are unmanned aerial vehicles (UAV's), including

missiles, reconnaissance and weapon delivery platforms, and test versions of access to space vehicles. Public acceptance of a UAV in sustained hypersonic flight under fully autonomous control, especially if it is a weapon or capable of delivering a weapon, would be unlikely. As such, if current hypersonic vehicle designs were to become operational they could not be tested at Edwards Air Force Base (or elsewhere) for the reasons sited above.

Air Force interest in pursuing a solution to telemetry through a plasma sheath has been renewed recently since the resulting methodology may dictate some hypersonic vehicle design requirements. (Note that the United States Air Force began researching solutions to telemetry through reentry plasma layers[1] in 1959.) The design of a hypersonic vehicle is a complex series of trade-offs between highly coupled systems, including, but not limited to, propulsion, control, volumetric, payload, fuel, structural, aerodynamic, mission, and telemetry requirements. One promising solution for allowing telemetry through plasma layers is through aerodynamic shaping of the vehicle leading edge to generate the desired plasma properties further downstream. Shaping of this type could possibly allow for telemetry at the tail of the vehicle with minimal signal attenuation. However, aerodynamic modification of a hypersonic vehicle after production would be more difficult and costly than redesigning the vehicle to account for the telemetry requirements in the beginning. As such, it is important to incorporate T&E concerns early in the vehicle design and mission selection phases so the requirements are accounted for when doing configuration studies. Therefore, solutions to radio frequency telemetry through a plasma sheath need to be researched before such vehicles get off of the drawing board or entire programs may fail due to an inability to safely do testing. This effort is further complicated by the fact that the degree of ionization and the resulting attenuation or blackout of telemetry signals is dependent on vehicle geometry, angle of attack, mission, flight velocity, and altitude.

II. HYPERSONIC FLOWFIELD

The attenuation of the radio frequency signals between a hypersonic vehicle enveloped in a plasma sheath and the ground stations, satellites, and aircraft tracking it can be severe and in most cases will be total during a portion of the flight. Although it is known that the mechanism of plasma generation is through the shock heating of the air above the molecular dissociation and ionization temperatures, the mechanism of how to control or modify the plasma is not sufficiently understood. The ionization problem can also be further complicated by the presence of ablation products in the flowfield.

In addition to propulsion, aerodynamic, and control issues, the ability to communicate through a plasma layer remains a critical area of research in hypersonic flight[2, 3, 4, 5, 6]. The accurate knowledge of vehicle position, velocity, flight path angle, and monitoring of overall vehicle health become especially important at hypersonic velocities. Due to the large velocity, a hypersonic vehicle has a tremendous amount of kinetic and potential energy as it travels through the atmosphere. At supersonic velocities, a shock wave is formed around the vehicle, thereby compressing and heating the oncoming air. At hypersonic velocities, this heating can be sufficient enough to increases the temperature above the dissociation and ionization temperatures of the air constituents, forming a plasma layer around the vehicle.

The plasma is an electrically charged gas consisting of both ionized molecules and free electrons and is often considered as the fourth state of matter. The dissociation of oxygen (above temperatures of about 2,000 K) and nitrogen (above temperatures of about 4,000 K) populates the plasma field with NO^+, N^+, and O^+ ions, along with neutralizing free electrons. In the most general sense, the term plasma refers to any electrically conducting gas regardless of the extent of ionization or degree of electrical neutrality associated with it. This layer of ionized gas between the

shockwave the vehicle is referred to as the plasma sheath. During the communication blackout portion of the flight the plasma is characterized by electron concentrations on the order of 10^{11} to 10^{16} electrons/m^3, depending on the configuration, flight velocity, trajectory, and location within the shock layer. It is the free electrons that attenuate or absorb the electromagnetic wave, especially when the transmission frequency is near to the plasma frequency. The plasma frequency is proportional to the square root of the electron density. Successful transmission through the plasma sheath will require transmission frequencies about the plasma frequency. Therefore, the solution to this problem will be achieved by lowering the electron density in the plasma sheath through aerodynamic shaping of the vehicle.

There are three dominant mission scenarios for which telemetry through a plasma sheath is a concern: 1) an air-breathing hypersonic cruise vehicle, 2) an access to space vehicle, and 3) a ballistic missile. Although these missions seem fundamentally different, the general physics involved in the electromagnetic wave/plasma sheath interaction are the same. The access to space vehicle and ballistic missile are designed to leave and subsequently reenter the earth's atmosphere. These types of vehicles could be traveling at velocities up to Mach 26 (about 8 km/s). An air-breathing access to space vehicle would spend much more of its flight within earth's atmosphere than a ballistic missile, and would likely be in a communication blackout for a significant amount of time. The air-breathing hypersonic cruise vehicle, which remains within the earth's atmosphere to provide oxidizer for its engine(s), also has the added concern that for a majority of its flight profile, the vehicle could be enveloped within a plasma sheath. The cruise vehicle can be envisioned as a missile, a weapon delivery platform, or a reconnaissance vehicle, and thus be traveling at any hypersonic Mach number. Current Air Force T&E concerns are to develop the ability to test air-breathing hypersonic cruise and access to space vehicles before the need arises.
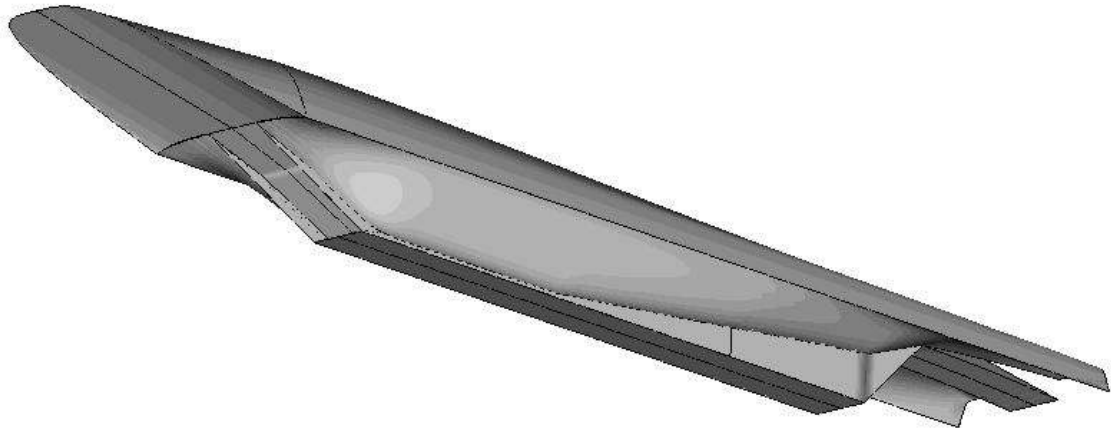
Figure 1: Air-breathing hypersonic missile concept. [8]

From as early on as the 1950's, research has been performed in the United States on solutions to the problem of telemetry through plasma layers, primarily for blunt body reentry vehicles[2, 7]. Much of this work provides insight into the ionized flowfield and particulars of the electromagnetic wave/plasma sheath interaction. Unfortunately, previous research generally focused on blunt body reentry vehicles, such as the Gemini and Apollo capsules, and blunted cones for ballistic missiles. Of the work that has been done in this area, little has been published in the open literature due to security concerns. Air-breathing hypersonic cruise and access to space vehicles currently being researched are designed with sharp leading edges to minimize losses due to drag[8], as shown by the missile in Figure 1. By building on the past work for blunt bodies under the unction of the necessity of sharp leading edge configurations, many benefits will be realized.

Vehicles at the reentry point in their trajectory are generally in a nose-up (high angle of attack) attitude in an effort to minimize surface heating. The surface heating increases inversely proportional to the square root of the radius (i.e., $q \propto R^{-1/2}$). By increasing the vehicle's effective leading edge radius for reentry there is a much more manageable heat load for the structure to

Figure 2: Dummy MIRV warheads on a Minuteman III Intercontinental Ballistic Missile (the left one has a modified sharp leading edge design as a part of the SHARP program at NASA Ames Research Center).

handle, which requires that more of the heat be absorbed by the air resulting in higher temperatures and a higher degree of ionization. Conversely, by reducing the effective leading edge radius, the electron concentration, and hence electromagnetic attenuation, is generally reduced (depending on the wave frequency) at the expense of increased localized heating at the leading edge. This localized heating for sharper leading edges has both advantages and disadvantages when considering telemetry through the plasma sheath; these details are explored on in the section on aerodynamic shaping.

Sample conical Multiple Independently Targetable Reentry Vehicles (MIRV) warheads launched from a Minuteman III Inter-Continental Ballistic Missile (ICBM) are shown in Figure 2. The two vehicles on the right in Figure 2 are the original design, while the one on the left has been modified with a sharp leading edge as part of the Slender Hypervelocity Aerothermodynamic Research Probes (SHARP) program[9, 10] at NASA Ames Research Center. Although not aimed at studying telemetry through plasma layers, the SHARP program is of considerable applicability since it is studying high temperature materials (hafnium diboride) that could be used to create leading edges with as low as 1 mm radius. As noted above, these sharper leading edges would have a dramatic impact on the reentry plasma and associated electron concentration.

A pictorial of the plasma sheath around a MIRV-type vehicle upon reentry is shown in Figure 3. There are five main regions used to characterize the flowfield around a decelerating hypersonic vehicle: stagnation region, intermediate region, aftbody region, wake region, and the boundary layer. Due to the unique nature of different vehicle configurations, the plasma electron density profile at any given location on a vehicle is a direct function of the vehicle shape, velocity, altitude, and angle of attack. Knowledge of the plasma electron density around a vehicle along with a better understanding of the characteristics for the different flowfield regions will allow for better design of the hypersonic vehicle to account for antenna type, placement, and utilization of communication blackout alleviation techniques.

The most severe plasma conditions exist in the stagnation region at the front of the vehicle. A nearly normal shock generates high temperatures and pressures in this region resulting in the highest levels of ionization. If the temperatures are high enough to ablate and ionize the leading edge material, then the electron concentrations would be higher than possible for pure air alone. As a result of these conditions, the vehicle antennas are placed as far from the stagnation region as possible where the environmental conditions are generally orders of magnitude less severe.
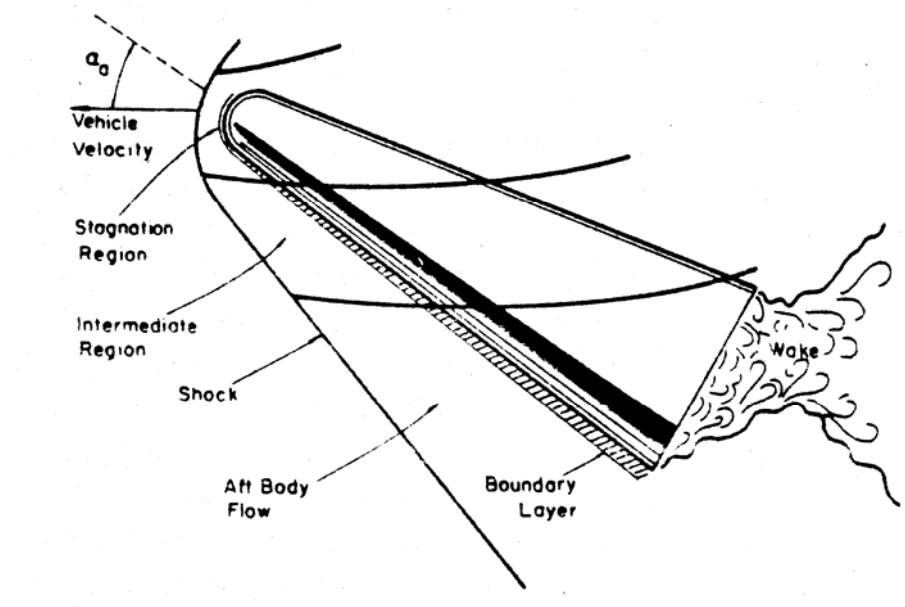
Figure 3: Flowfield around a representative conical reentry vehicle.[3]

The intermediate region, which follows the stagnation region, is characterized by the plasma in a state of chemical nonequilibrium. Although the conditions in this region are not as severe as in the stagnation region, the communications blackout experienced by aft-mounted antennas are caused by this region if the vehicle is at a moderate angle of attack. If a high angle of attack is used, then the blackout is caused mainly by the aftbody region (depending on the flowfield streamlines). A hypersonic cruise or ascending access to space vehicle will generally be at a very low angle of attack.

The plasma flowfield in the aftbody region is developed mostly by the flow whose streamlines pass through the oblique shock and flow past the aftbody. Correspondingly, the plasma conditions in this region are much less severe than the conditions in the intermediate region.

At the base of the vehicle, the flow in the wake region exhibits a complex structure consisting of separated flow, circulation, and a large amount of electron ion recombination over

part of the rear, and frozen flow over the other part. The plasma in this region generally will not affect communication if the frequency is greater than 1 GHz. If the flowfield is significantly contaminated with ablation products then there will be an effect on communication, even at frequencies greater than 1 GHz. For an air-breathing hypersonic vehicle, the base region would have a more tapered profile, as shown in the missile in Figure 1.

The final flow regime is the viscous boundary layer, which exists along the entire surface of the vehicle and is therefore part of each of the other four regions to some extent. As is characteristic of any boundary layer, large gradients in both temperature and velocity exist. Boundary layer ionization, in reference to signal attenuation, is only significant above an altitude of about 75 km where the boundary layer thickness is similar to the thickness of the shock layer. The properties in the inviscid region outside of the boundary layer generally have a much more significant effect on signal strength at lower altitudes. Therefore, the effects of ionization in the boundary layer are frequently neglected in signal attenuation calculations.

For the type of MIRV pictured in Figure 2 and Figure 3, the plasma sheath exists between altitudes of 120 km down to 15 km with the peak electron density occurring at about 27 km. Sample contours showing the calculated radial distribution of electron density and collision frequency at the antenna location (near the rear of the vehicle) are shown in Figure 4. The corresponding temperature profile is nonlinear and ranges from about 3,800 K at the vehicle surface to about 2,000 K at the shock wave. From Figure 4 it can be clearly seen that the collision frequency in this region near the rear of the vehicle is fairly linear while the electron density is highly nonlinear.
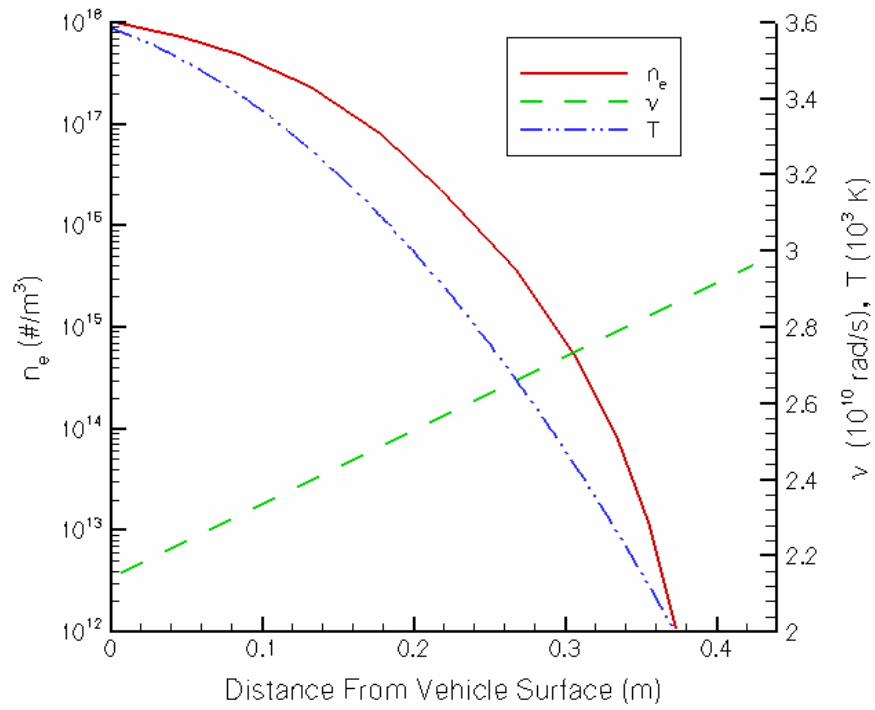
Figure 4: Radial electron density and collision frequency profiles at the antenna location on a typical blunt-nosesd MIRV at 27 km.[3]

III. ACTIVE APPROACHES FOR REDUCING COMMUNICATION ATTENUATION AND BLACKOUT

From the beginning of man's ventures into space, many different methodologies for actively reducing the plasma sheath effects on radio communication attenuation and blackout have been proposed and studied. Due to the fact that military requirements for the ability to communicate through plasma layers during reentry remains an important research topic, most of the experimental results in this area are classified and thus not published in the open literature. Despite this, a good understanding of the breadth of current research areas is still possible, as they have changed little in the last 40 years. Since the understanding and experience with atmospheric reentry and its associated aerodynamic environment and communication problems have increased, there is promise that a reliable solution will be found. Of the methods which have been flight tested and had positive results, the decision of implementation remains with the vehicle designers regarding trade-offs for system weight, power, reliability, and infrastructure requirements. Also, the degree of importance to which the ability to alleviate blackout plays in the overall system will determine if vehicle configuration changes and associated aerodynamic and control penalties are warranted. The most promising areas of research for actively reducing communication attenuation and blackout to be discussed in this report are: low frequency transmission, high frequency transmission, use of an aerodynamic gas spike, electrophilic injection, and use of magnetic fields. The applicability of any of these methods depends in part on its success in reducing or alleviating the communications blackout and in part on the geometry, velocity, and angle of attack of the reentry vehicle in question. Some methods would be better for smaller vehicles while others show more promise for larger manned reentry vehicles. The requirements for or effectiveness of any of these methods may

be severely altered through aerodynamic shaping and altering of the reentry plasma,[11,12] as was discussed above.

1. Low Frequency Transmission

The attenuation of low frequency electromagnetic waves in the plasma environment decreases significantly for transmission well below the plasma resonance frequency. Microwave transmissions are typically below the plasma frequency so this method allows the use of existing telemetry infrastructure.

2. High Frequency Transmission

What would seem the simplest solution to the communication blackout problem is to use radio frequencies well above the plasma frequencies (i.e., ω >10 GHz). This was discounted as a feasible solution in the past due to the weight of the then state-of-the-art systems and the associated infrastructure cost of installing this type of equipment at tracking stations or the development and launch of a satellite network. Recent advances in satellite systems make this a much more viable option. NASA is currently launching the second of a new series of three advanced tracking and data relay satellites (TDRS-I).[13] The TDRS constellation will contain a total of 10 satellites when completed. The satellites provide communication abilities in the S-band (2.0 to 2.3 GHz), Ku-band (13.7 to 15.0 GHz), and Ka-band (22.5 to 27.5 GHz). As systems of this sort become more commonplace, both in satellites and on the ground, the solution to telemetry through plasma layers for most situations will most likely become high frequency transmission. The question or concern will then be whether or not you have satellite coverage in the required test or flight range.

3. Electrophilic Injection

Numerous studies have been performed, both experimentally and in flight tests, for the reduction of electron concentrations in plasma sheaths using electrophilic injection upstream of the antenna. The plasma frequency is lowered by the recombination of free electrons to electrophilic materials, which form negative ions. Tests of a wide variety of different materials have been tried including solids,[14] liquids,[15] and gases.[16] The most promising are liquids because they are easiest to inject with reasonable penetration into the plasma layer. The most successful tests were part of the Mercury, Gemini, [3] and Radio Attenuation Measurements[11,12] (RAM) programs, which all showed positive blackout alleviation at a variety of test conditions for very different configurations, velocities, and plasma conditions. The downside to this method is the extra equipment and fluid volume and weight penalties to meet the high mass flow rates required (on the order of kilograms per second) to reduce the electron concentration.

Many researches have also looked at the concept of an aerodynamic gas spike not only as a means of reducing aerodynamic drag and heating for reentry vehicles,[1,17] but also at low hypersonic Mach numbers.[18] This method remains problematic due to injector penetration, cooling, vehicle interaction, and applicability in a very small angle of attack corridor.

4. Magnetic Fields

An elegant technique for alleviating the blackout transmission problem is through the use of a magnetic field to create a 'spectral window' through which telemetry signals can pass with little to no attenuation. The methods mentioned above either reduce the electron concentration in the plasma sheath or require transmission at frequencies away from the plasma resonant frequency where there is less attenuation. This method superimposes a static magnetic field B onto the plasma

thereby altering the electromagnetic properties. For increasing magnetic field strength, the transverse motion of the electrons decreases. In the limit of an infinitely strong magnetic field no interaction will take place between the electrons and an electromagnetic plane wave whose wave front is normal to B. For finite values of B the frequency band where this method is applicable becomes constrained. Theoretical[19] and experimental[20] work focused on transmission frequencies below the plasma resonance frequency. Of course, this method falls prey to the weight and operational constraints for superconducting magnets and their associated cryogenic systems. It is suggested that this method would not be practical for large vehicles where the magnetic field lines would need to extend through thick plasma layers. For smaller vehicles it is suggested that aerodynamic shaping coupled with proper transmission frequency selection would reduce the need for any sort of magnetic field device.

One analytical study by Hodara in 1961 claimed successful transmission up to about 1 GHz without attenuation through a collisionless plasma with density of 10^{15} electrons/m^3 using a 0.036 Tesla static magnetic field. Although this is an idealized scenario, further analysis and experimental work cited by Hodara claimed favorable results. It was proposed that a magnetic field of this magnitude could be successfully created using a 16 kg, 1,000-turn spiral coil of no. 10 aluminum wire. The system used a standard 28-volt dc source, dissipated about 150 watts, and generated a 0.05 Tesla field at the boundary layer (where the highest electron concentration existed in the plasma sheath).

5. Aerodynamic Shaping Effects

With a general description of the plasma physics and aerodynamics of hypersonic reentry vehicles complete, the benefits of aerodynamic shaping of the vehicle can be explored. As was shown in Figure 1 and Figure 2, there is considerable interest and research which pertains to sharp

leading edge hypersonic configurations. This is primarily due to the drag reduction and lift increase that can be achieved by having a sharper leading edge with an attached shock wave. Unfortunately, sharper leading edge vehicles also have associated problems, such as a higher leading edge heat transfer rate. Also, for a given length vehicle, increasing the sharpness of the leading edge will decrease both the vehicle volume and volumetric efficiency.

As mentioned above, an air-breathing hypersonic cruise vehicle will only use a small range of angle of attack. Thus, the cruise vehicle flowfield will be different than was described for the reentry bodies, but by understanding the advantageous results from the reentry flowfield, the cruiser can be shaped to provide similar properties. The reentry bodies generally try to locate the telemetry antenna towards the back of the vehicle in the aftbody flow region. An air-breathing vehicle also requires placement of the antenna as far from the stagnation region as possible, but due to the small angles of attack in this case, the vehicle flowfield will be dominated by streamlines passing through the stagnation region. Therefore, the challenge of aerodynamic shaping is in designing the vehicle to minimize the flowfield temperature (and hence, lower the electron concentrations) while ensuring the structural viability of the leading edge.

The flowfield generated at the leading edge is extremely important for an air-breathing hypersonic vehicle since a streamline that originates at the leading edge will generally pass by the tail of the vehicle. By using a sharp leading edge on a hypersonic vehicle, not only will the temperatures be lower than if the leading edge was blunt, but the plasma sheath surrounding the vehicle will be thinner and contain fewer free electrons. The benefit of a thinner plasma sheath is that it will be easier to transmit through or easier to alter using an active method of plasma modification.[7] By thinning the shock layer, however, the temperature and electron gradients will be more severe than shown for the blunt body in Figure 4.

.

The relative effects of reducing the leading edge radius are understood, but what requires further investigation is to determine the optimum shape for the leading edge. Generally, simple circular cylinder shapes are used for leading edges, but research has shown that it is possible to generate non-circular, sharp leading edges that may provide a more advantageous telemetry environment.[21,22] There is a class of leading edge shapes, generated by a two-dimensional power law function ($y=Ax^n$), which show a desirable combination of aerodynamic and geometric properties. Certain designs behave aerodynamically sharp (attached shock), while simultaneously behaving geometrically blunt (good heat transfer characteristics). These power law shaped leading edges show promise towards providing a more benign plasma environment.

By shaping the vehicle geometry in the proper fashion, it may be possible to design the shock layer so it expands rapidly after the flow is past the leading edge. By rapidly expanding the flow, the temperature will be reduced, and along with it, possibly the electron concentration (through recombination with the ionized species). If expanded too rapidly, the temperature will drop too quickly and the flow will freeze (i.e., chemical reactions will cease and the ion and electron concentrations will be fixed). These recombination and freezing characteristics have been studied for reentry bodies,[23,24] but further work is needed to generate methodologies for advantageous aerodynamic shaping of sharp leading edge, air-breathing hypersonic vehicles.

IV. ELECTROMAGNETIC WAVE INTERACTION WITH A MAGNETOACTIVE PLASMA SHEATH

With a general understanding of the type of flowfield a reentry vehicle might encounter and approaches which could be applied to reducing the interaction between an electromagnetic wave and a plasma sheath, a mathematical framework of the problem of communication blackout must be developed. This will lead to solutions to possible alleviation of the signal attenuation associated with the interaction between an electromagnetic wave and a magnetoactive plasma sheath.

A simple, but reasonable analysis for understanding the reflection and attenuation of electromagnetic waves caused by free electrons can be developed analytically.[3,25] The plasma is assumed to be charge balanced (i.e., an equal number of free electrons and positive ions exist) and to contain some neutral particles. The average equilibrium separation between the charged particles is maintained as a result of their electrostatic fields. The movement of one of the charged particles (with all others remaining fixed) about its equilibrium position can be modeled as a damped spring-mass system. The spring is the restoring intermolecular electrostatic force, the mass is the displaced particle, and the damping is provided by the collisions between the neutral particles and the oscillating charged particle. The plasma electron frequency ω_p, commonly referred to as the plasma frequency, is the natural frequency at which the free electron oscillates in the presence of a plasma.[25,26]

$$\omega_p \equiv \sqrt{\frac{n_e e^2}{\varepsilon_0 m_e}} \approx 56.416\sqrt{n_e} \tag{1}$$

where n_e is the electron density, e is the electronic charge (-1.602×10^{-19} C), ε_0 is the permittivity (dielectric constant) of free space ($10^7/4\pi c^2$ F/m), m_e is the electron mass (9.107×10^{-31} kg), and c is the speed of light (3×10^8 m/s). The plasma frequency for electrons is directly proportional to the

square root of the electron density. The plasma frequency can also be converted to Hertz by $f_p = \omega_p / 2\pi$. The plasma ion frequency ω_i is represented by an equation identical in form to Equation 1, with a positive ion having an integer multiple (depending on the degree of ionization) of the electron charge, only opposite in sign. The ion plasma frequency is much smaller than the electron plasma frequency because the ion mass is generally about four orders of magnitude larger than the electron mass. Therefore, the effects of the ion plasma frequency will be neglected in this analysis.

The propagation of an electromagnetic wave through a plasma field is described by the Maxwell equations. Additionally, the equations of motion, assuming a sinusoidal steady-state (time-harmonic) solution with $e^{j\omega t}$ time dependence, are necessary. The phasor form of the Maxwell equations for this system are:

$$\nabla \times \mathbf{H} \cong j\omega\varepsilon_0\mathbf{E} + N_e q_e \mathbf{v} \tag{2}$$

$$\nabla \times \mathbf{E} \cong -j\omega\mu_0\mathbf{H} \tag{3}$$

$$\nabla \cdot (\varepsilon_{\text{eff}}\mathbf{E}) = 0 \tag{4}$$

$$\nabla \cdot \mathbf{H} = 0 \tag{5}$$

The equations of motion governing electrical and magnetic forces acting upon a charged particle are described by the Lorentz force equation

$$\begin{aligned}
\overline{F}_{\text{elec}} + \overline{F}_{\text{mag}} &= q_e\overline{E} + q_e\widetilde{\mathbf{v}} \times (\mathbf{B}_0 + \overline{B}) \\
&= q_e\left[\overline{E} + \widetilde{\mathbf{v}} \times (\mathbf{B}_0 + \overline{B})\right]
\end{aligned} \tag{6}$$

where $\overline{F}_{\text{elec}}$ and $\overline{F}_{\text{mag}}$ are the electrical and magnetic Lorentz forces, respectively. The electron velocity is given by $\widetilde{\mathbf{v}}$, an applied steady magnetic field by $\mathbf{B}_0$, and the electric and magnetic fields of the incident electromagnetic wave are given by $\overline{E}$ and $\overline{B}$, respectively. Recall that the electron charge q_e is a negative quantity.

For a lossy plasma, the viscous forces accounting for the momentum loss due to molecular interactions are included

$$\overline{\mathbf{F}}_{visc} = -m_e \nu \, \tilde{\mathbf{v}} \tag{7}$$

where ν is the electron collision frequency (assumed to be independent of velocity). The acceleration of the charged particle is then given by Newton's second law

$$\overline{\mathbf{F}} = \frac{d(m_e \tilde{\mathbf{v}})}{dt} \tag{8}$$

resulting in the equations of motion for charged particles in a plasma field in the presence of an applied magnetic field

$$\frac{d(m_e \tilde{\mathbf{v}})}{dt} = q_e \left[\overline{\mathbf{E}} + \tilde{\mathbf{v}} \times (\mathbf{B}_0 + \overline{\mathbf{B}}) \right] - m_e \nu \, \tilde{\mathbf{v}} \tag{9}$$

Assuming all field quantities vary harmonically in the form

$$\tilde{\mathbf{v}} = \Re\left\{ \mathbf{v} e^{j\omega t} \right\} \tag{10}$$

and neglecting second order interaction effects results in the phasor form of the equations of motion

$$j\omega \, m_e \mathbf{v} \cong q_e \left[\mathbf{E} + \mathbf{v} \times \mathbf{B}_0 \right] - m_e \nu \, \tilde{\mathbf{v}} \tag{11}$$

Rearranging terms and explaining components in the form $[\mathbf{A}]\mathbf{v} = \mathbf{E}$ results in

$$\begin{bmatrix} (C_1 C_2)^{-1} & -B_{0z} & B_{0y} \\ B_{0z} & (C_1 C_2)^{-1} & -B_{0x} \\ -B_{0y} & B_{0x} & (C_1 C_2)^{-1} \end{bmatrix} \begin{bmatrix} v_x \\ v_y \\ v_z \end{bmatrix} = \begin{bmatrix} E_x \\ E_y \\ E_z \end{bmatrix} \tag{12}$$

where the scalar coefficients C_1 and C_2 are

$$C_1 = -\frac{q_e}{m_e} \tag{13}$$

$$C_2 = \frac{j}{(\omega - j\nu)} \tag{14}$$

Equations 12 are then solved for the velocity vector in the form

28

$$\mathbf{v} = C_1 C_3 [\mathbf{A}]^{-1} \mathbf{E} \tag{15}$$

where $[\mathbf{A}]^{-1}$ is the inverse of matrix $[\mathbf{A}]$ and C_1 and C_3 are scalars, resulting in

$$\begin{bmatrix} v_x \\ v_y \\ v_z \end{bmatrix} = C_1 C_3 \begin{bmatrix} A_{11}^{-1} & A_{12}^{-1} & A_{13}^{-1} \\ A_{21}^{-1} & A_{22}^{-1} & A_{23}^{-1} \\ A_{31}^{-1} & A_{32}^{-1} & A_{33}^{-1} \end{bmatrix} \begin{bmatrix} E_x \\ E_y \\ E_z \end{bmatrix} \tag{16}$$

where the electric field coefficients are given by

$$A_{11}^{-1} = \omega_{cx}^2 + 1/C_2^2 \tag{17}$$

$$A_{12}^{-1} = \omega_{cx}\omega_{cy} + \omega_{cz}/C_2 \tag{18}$$

$$A_{13}^{-1} = \omega_{cx}\omega_{cz} - \omega_{cy}/C_2 \tag{19}$$

$$A_{21}^{-1} = \omega_{cx}\omega_{cy} - \omega_{cz}/C_2 \tag{20}$$

$$A_{22}^{-1} = \omega_{cx}^2 + 1/C_2^2 \tag{21}$$

$$A_{23}^{-1} = \omega_{cy}\omega_{cz} + \omega_{cx}/C_2 \tag{22}$$

$$A_{31}^{-1} = \omega_{cx}\omega_{cz} + \omega_{cy}/C_2 \tag{23}$$

$$A_{32}^{-1} = \omega_{cy}\omega_{cz} - \omega_{cx}/C_2 \tag{24}$$

$$A_{33}^{-1} = \omega_{cx}^2 + 1/C_2^2 \tag{25}$$

$$C_3 = \frac{C_2}{\omega_c^2 + 1/C_2^2} \tag{26}$$

and the electron cyclotron frequency (or gyro-frequency) is defined as

$$\omega_c = -\frac{q_e}{m_e}\mathbf{B}_0 = C_1\mathbf{B}_0 = \omega_{cx}\hat{\mathbf{x}} + \omega_{cy}\hat{\mathbf{y}} + \omega_{cz}\hat{\mathbf{z}} \tag{27}$$

With the velocity vector now determined we can proceed to alter Maxwell's equations to construct the electromagnetic field. Starting by taking the curl of Equation 3

$$\nabla \times (\nabla \times \mathbf{E}) = \nabla \times (-j\omega\mu_0\mathbf{H}) \tag{28}$$

and then substituting the result into Equation 2 results in the description of the electric field $\mathbf{E}$ as a function of the electron velocity $\mathbf{v}$.

$$\begin{aligned}
\nabla \times (\nabla \times \mathbf{E}) &= -j\omega\mu_0 (j\omega\varepsilon_0 \mathbf{E} + N_e q_e \mathbf{v}) \\
&= \omega^2 \mu_0 \varepsilon_0 \mathbf{E} - j\omega\mu_0 N_e q_e \mathbf{v}
\end{aligned}$$
(29)

Equation 29 can be further simplified by using the vector identity

$$\nabla \times (\nabla \times \mathbf{E}) = \nabla(\nabla \cdot \mathbf{E}) - \nabla^2 \mathbf{E}$$
(30)

and the definition of wave number

$$k_0 = \frac{\omega}{c} = \frac{\omega}{\sqrt{\varepsilon_0 \mu_0}}$$
(31)

where the phase velocity in a vacuum is the speed of light. Substituting $\mathbf{v}$ from Equation 16 results in the wave equation for the interaction between an electromagnetic wave and a plasma field in the presence of a static magnetic field.

$$\nabla^2 \mathbf{E} + \frac{k_0^2}{\varepsilon_0} \varepsilon_{\text{eff}}^{ij} \mathbf{E} = 0$$
(32)

The coefficient of the electric field vector $\varepsilon_{\text{eff}}^{ij}$ is the effective dielectric tensor which is a product of the freestream dielectric constant and the relative dielectric tensor

$$\varepsilon_{\text{eff}}^{ij} = \varepsilon_0 \varepsilon_r^{ij} = \varepsilon_0 \left([\mathbf{I}] + j\frac{\omega_p^2}{\omega} C_3 [\mathbf{A}]^{-1} \right)$$
(33)

Case 1. External Magnetic Field Absent

An understanding of the general interaction between an incident electromagnetic wave and a reentry plasma sheath can be obtained by setting the external magnetic field strength to zero (i.e., $\mathbf{B}_0 = 0$). This results in all of the electron cyclotron frequencies given in Equation 27 to be set to zero in Equation 32. The simplified wave equation is then given by

$$\nabla^2 \mathbf{E} - \gamma_p^2 \mathbf{E} = 0 \tag{34}$$

where the propagation constant γ_p is given by

$$\gamma_p^2 = k_0^2 \varepsilon_r^{ij} \tag{35}$$

It can be seen that for this case without the applied magnetic field, Equation 34 reduces to three scalar equations since the relative dielectic tensor becomes

$$\varepsilon_r^{ij} = \begin{bmatrix} \varepsilon_r' - j\varepsilon_r'' & 0 & 0 \\ 0 & \varepsilon_r' - j\varepsilon_r'' & 0 \\ 0 & 0 & \varepsilon_r' - j\varepsilon_r'' \end{bmatrix} \tag{36}$$

where ε_r' and ε_r'' are the real and imaginary parts of the relative dielectric scalar, respectively.
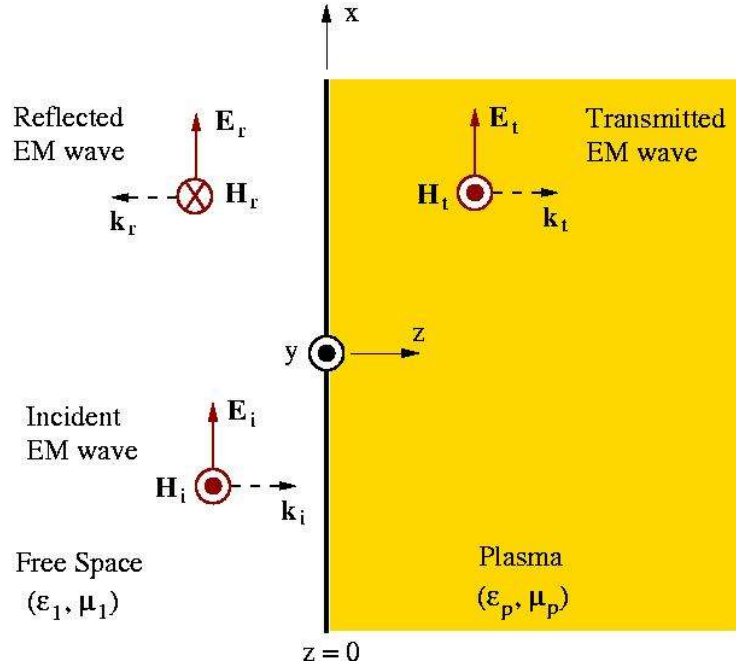

Figure 5: Electromagnetic wave interaction with a plasma boundary (normal incidence).

$$\varepsilon'_r = 1 - \frac{\omega_p^2}{\omega^2 + \nu^2} \tag{37}$$

$$\varepsilon''_r = \frac{\omega_p^2 \, \nu/\omega}{\omega^2 + \nu^2} \tag{38}$$

Therefore, for a linearly polarized, uniform plane wave propagating perpendicular to the plasma face $\mathbf{E} = E_x e^{-\gamma_p z} \hat{\mathbf{x}}$, as shown in Figure 5, the propagation constant is given by

$$\gamma_p = jk_0 \sqrt{\varepsilon'_r - j\varepsilon''_r} = \alpha_p + j\beta_p \tag{39}$$

where α_p and β_p are defined as the plasma attenuation and phase constants, respectively. These constants are given by

$$\alpha_p = k_0 \left[\frac{\sqrt{\varepsilon'^2_r + \varepsilon''^2_r} - \varepsilon'_r}{2} \right]^{1/2} \tag{40}$$

and

$$\beta_p = k_0 \left[\frac{\sqrt{\varepsilon'^2_r + \varepsilon''^2_r} + \varepsilon'_r}{2} \right]^{1/2} \tag{41}$$

respectively.

Solution A: Collisionless Plasma

Using Equations 40 and 41, the special case of an electromagnetic wave propagating in a collisionless plasma (i.e., $\nu = 0$) can be considered. In this instance, both the attenuation factor α_p and the imaginary part of effective dielectric coefficient ε''_r are identically equal to zero resulting in a propagation factor of

$$\gamma_p = jk_0 \sqrt{\varepsilon'_r} = jk_0 \sqrt{1 - \frac{\omega_p^2}{\omega^2}} \tag{42}$$

Therefore, for a wave frequency ω greater than the plasma frequency ω_p, the wave propagates without attenuation. When ω is less than ω_p, the electric field is given by an exponentially decaying wave. If $\omega = \omega_p$ then ε'_r is also zero and the electromagnetic wave is totally reflected at the surface and does not propagate into the plasma.

Solution B: Lossy Plasma

The simple distinctions which were made above for a lossless plasma do not hold when the electron collision frequency becomes significant. For this lossy plasma case (i.e., $\nu \neq 0$), the value of ε''_r exists at all frequencies. Therefore, the plane wave will propagate with attenuation for all cases, as given by Equations 40 and 41. The results for Equations 40 and 41 are plotted in Figure 6 and Figure 7, respectively. The results are plotted in terms of normalized transmission frequency ω/ω_p and normalized electron collision frequency ν/ω_p.

As was eluded to in the previous section for low frequency transmissions (much below the plasma frequency), there is some transmission benefit which can be realized, although really only when the normalized collision frequency exceeds unity. Generally, as the wave frequency increases above the plasma frequency, the attenuation factor α_p decreases rapidly prompting a desire for large values of ω. This was referred to as high frequency transmission.
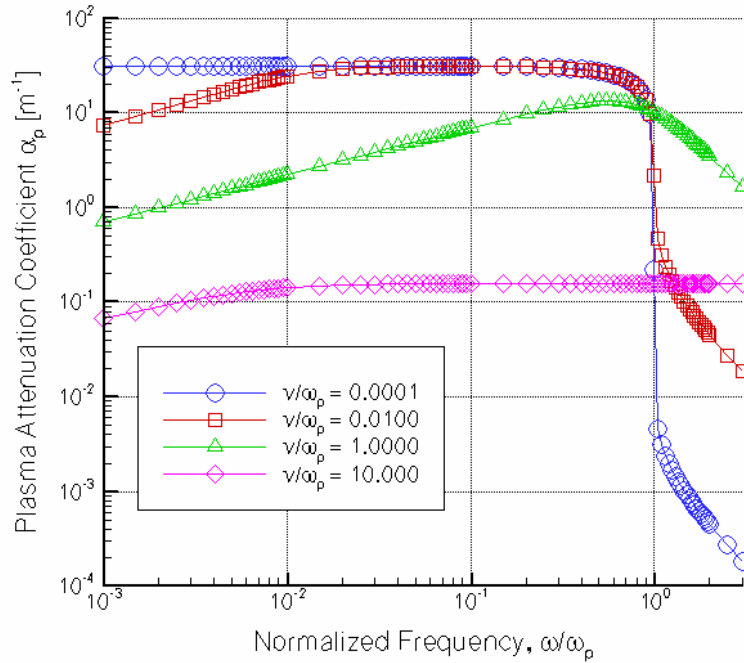
Figure 6: Plasma attenuation constant versus normalized transmission frequency for a range of normalized collision frequencies. There is no applied magnetic field in these cases ($B_0 = 0$).
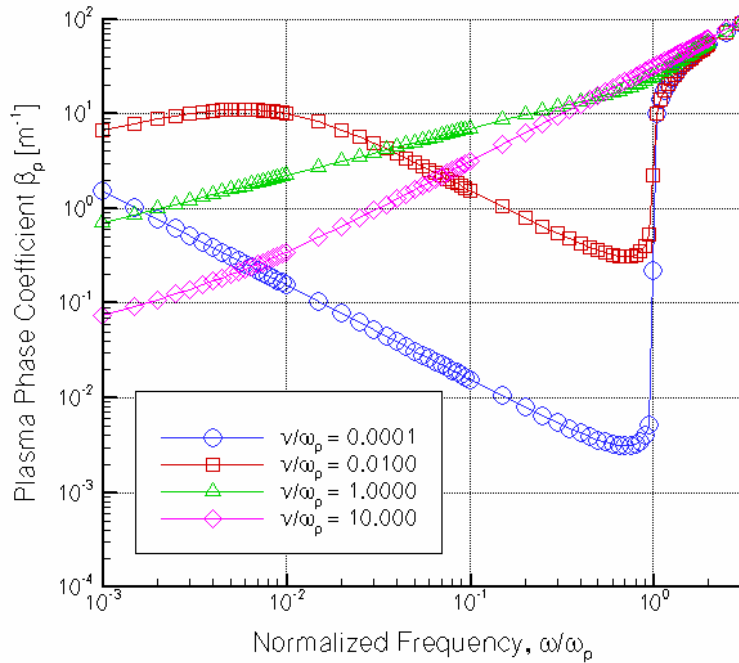

Figure 7: Plasma phase constant versus normalized transmission frequency for a range of normalized collision frequencies. There is no applied magnetic field in these cases ($B_0 = 0$).

Case 2: Applied Magnetic Field Normal to Plasma Layer Interface

One problem where Equation 32 reduces to a simplier form is when the static magnetic field is aligned with one of the coordinate directions, such as $\mathbf{B}_0 = B_{0z}\hat{\mathbf{z}}$ (i.e., normal to the plasma interface). This corresponds to setting the electron cyclotron frequencies $\omega_{cx} = \omega_{cy} = 0$.

The solution to the wave equation (Equation 32) can be determined by making some assumptions for the wave polarization. Since linearly polarized waves (i.e., $\mathbf{E} = E_x(z)\hat{\mathbf{x}}$) are not possible solutions in a plasma with a static magnetic field ($\mathbf{B}_0 \neq 0$), the solution requires the use of circularly polarized waves. Similar to what was shown in Figure 4, circularly polarized waves propagating in the $\hat{\mathbf{z}}$ direction are expressed by

$$\mathbf{E} = E_0(\hat{\mathbf{x}} \mp j\hat{\mathbf{y}})e^{\gamma_p z} \tag{43}$$

where the negative and positive signs indicate right hand circularly polarized (RHCP) and left hand circularly polarized (LHCP) waves, respectively.

The attenuation and phase constants for the normal magnetic field case are shown in Figure 8 and Figure 9 for the RHCP waves (superscript +) and in Figure 11 and Figure 10 for the LHCP waves (superscript −). It becomes very clear that as the normalized collision frequency ν/ω_p decreases (towards the lossless plasma limit) that there is much less attenuation in the transmission.

The range of normalized frequencies ω/ω_p for which the transmission is cutoff are decreased by increasing the magnetic field strength for the RHCP waves. For the LHCP waves this is also true, but telemetry only becomes realizable for frequencies approximately greater than the plasma frequency.
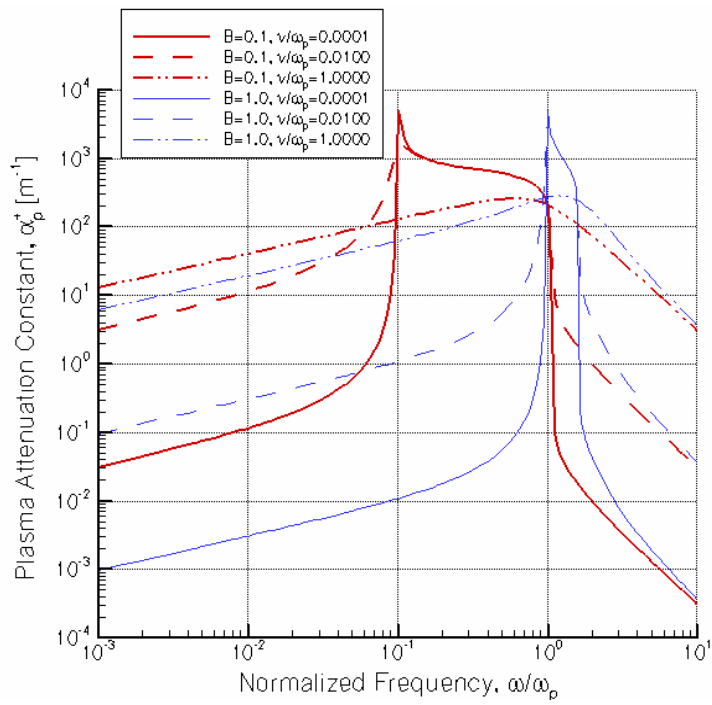
Figure 8: Plasma attenuation constant (RHCP) versus normalized transmission frequency for a range of normalized collision frequencies and normal magnetic field strengths.

Figure 9: Plasma phase constant (RHCP) versus normalized transmission frequency for a range of normalized collision frequencies and normal magnetic field strengths.

Figure 11: Plasma attenuation constant (LHCP) versus normalized transmission frequency for a range of normalized collision frequencies and normal magnetic field strengths.
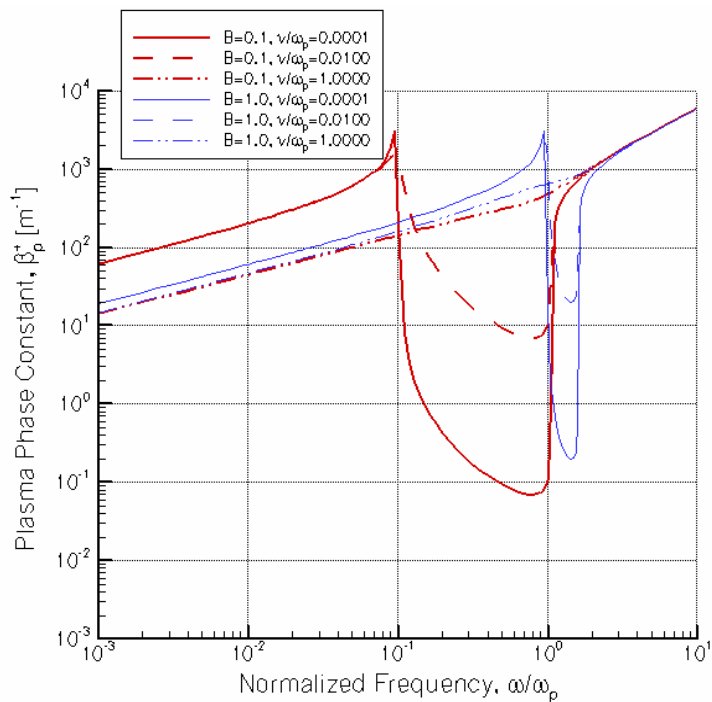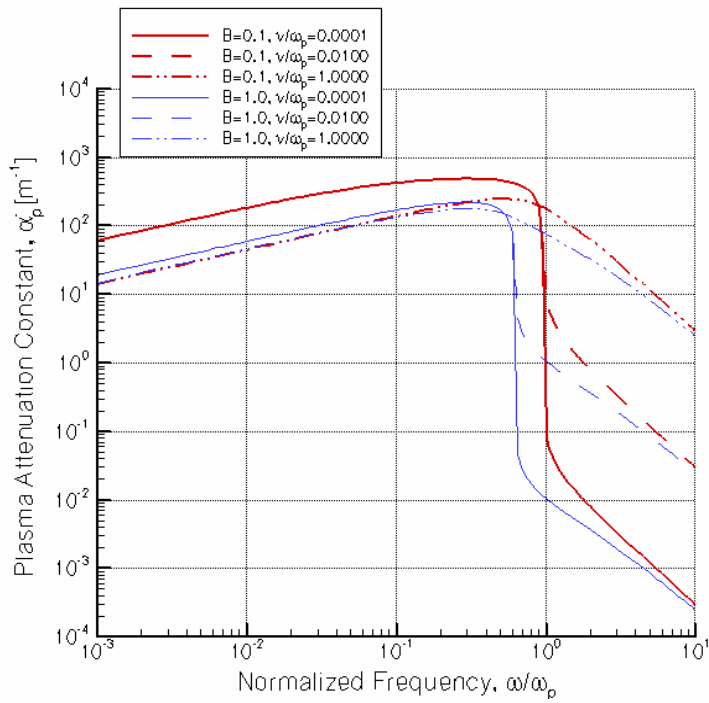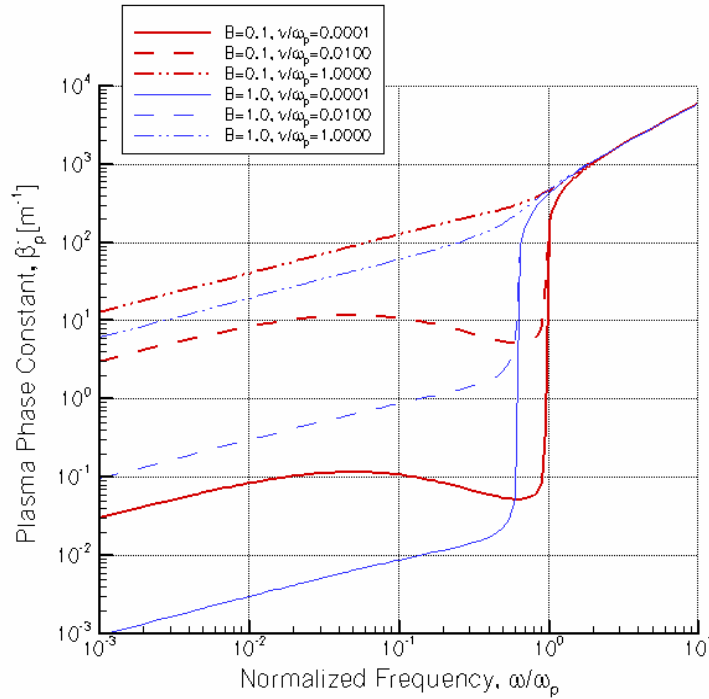

Figure 10: Plasma phase constant (LHCP) versus normalized transmission frequency for a range of normalized collision frequencies and normal magnetic field strengths.

Through vehicle shaping effects (sharper leading edges) the plasma frequency can be lowered allowing for possible transmission at high frequencies $(\omega > \omega_p)$ where the attenuation is lowered. Also, through sharper leading edges, the collision frequency should be lowered (lower temperatures and pressures) creating a plasma environment closer to the lossless limits.

As an example, the plasma conditions associated with the MIRV vehicle shown in Figure 2 and Figure 3 can be examined. For microwave range transmission ($f = 2.45$ GHz, $\omega = 15.39 \times 10^{10}$ rad/s), the surface of the MIRV vehicle has a plasma frequency of $\omega_p = 5.64 \times 10^{10}$ rad/s and a normalized collision frequency of $\nu/\omega_p = 0.39$. The normalized transmission frequency is $\omega/\omega_p = 0.273$. Within the limits of this analysis it becomes clear that with a RHCP wave and $\mathbf{B}_0 = 0.1$ T magnetic field that a microwave transmission will be close to the cutoff frequency. Of course, a stronger magnetic field would reduce this possibility, but at the added expense of extra power, volume, and weight on an already tiny vehicle. The LHCP wave would require much stronger magnetic fields to be useful in this scenario.

V. COMPARISON WITH BLACKOUT FLIGHT DATA

Using the methodologies defined above for solving the steady, inviscid, nonequilibrium plasma flow through shock waves to determine the electron concentration and attenuation constant (Equation 2), the space shuttle orbiter and RAM C-II flight tests were examined. Figure 12 shows the space shuttle blackout trajectory while Figure 13 shows the RAM C-II blackout trajectory. The plasma attenuation coefficient $\alpha_p = 1$ for nonequilibrium flow through shock waves are plotted as contour lines for various wedge angles using the peak electron concentration. The right side of each contour line is the blackout area and the left side is where telemetry can take place.

It should be noted that errors in the calculations are evident at both high and low altitudes where the peak electron concentrations will likely never be reached due to velocity and pressure effects, respectively. At higher altitudes the mean free path will become sufficiently large where continuum modeling of the flow is inaccurate and a Direct Simulation Monte Carlo (DSMC) methodology should be used. Also, the collision frequency was set equal to the electron production rate which is an underestimation of ν since each collision does not necessarily result in an ionization or recombination reaction taking place.
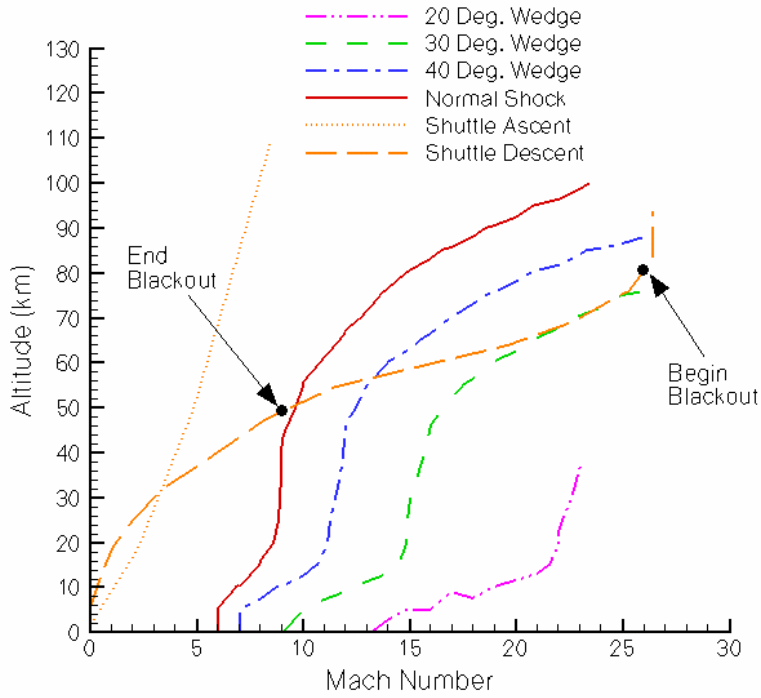
Figure 12: Blackout points along the reentry trajectory for the space shuttle orbiter along with plasma attenuation coefficient unity lines for various wedge angles.
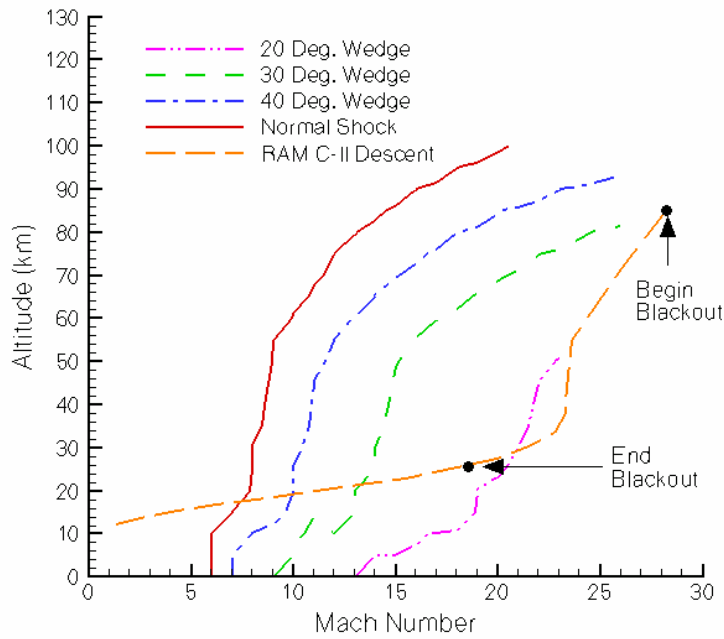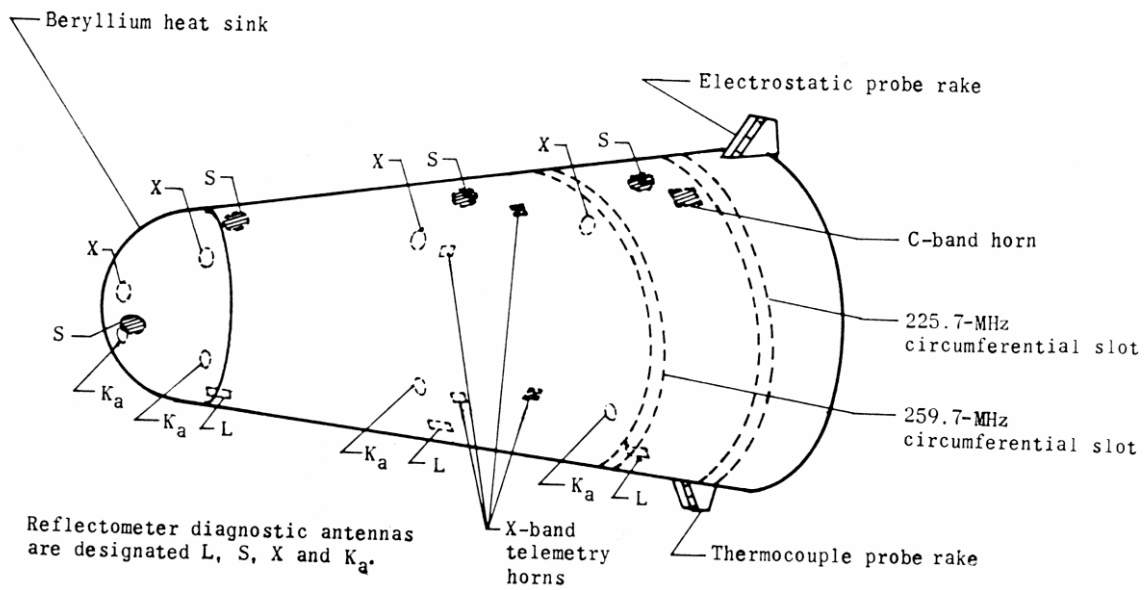

Figure 13: Blackout points along the reentry trajectory (from Ref. 19) for the RAM C-II flight test vehicle along with plasma attenuation coefficient unity lines for various wedge angles.

Reflectometer diagnostic antennas are designated L, S, X and K_a.

Space Shuttle Orbiter

The space shuttle orbiter ascent and descent trajectories along with the known blackout start and termination points are shown in Figure 12. The shuttle orbiter transmits at a frequency $f = 2.1064$ GHz and has an angle of attack of about 40° throughout its 16 minute blackout. During its reentry the orbiter uses a large number of "S-turns" to slowly dissipate energy. It is likely that the unsteady effects from the turning in combination with the high altitude velocity effects mentioned above contribute to the shuttle exhibiting the effective attenuation coefficient equivalent to a 30° wedge during the deceleration from Mach 26 to Mach 18. After this point the effective attenuation coefficient steadily increases from a 30° wedge equivalent (at Mach 18) to a flat plate equivalent (at

Mach 9), where the shuttle emerges from blackout. It is through this second part of the reentry that the shuttle transitions from a slender body approximation to a blunt body, flat plate flowfield This indicates that the stagnation flow region on the shuttle is exhibiting greater influence on the telemetry mechanism, most likely due to boundary layer, and frozen flow effects.

Radio Attenuation Measurements C-II Flight Test Vehicle

Begin a much more slender body, the RAM C-II flight test vehicle will have a much more viscous dominated plasma sheath, with higher electron concentrations than calculated here using Euler equations. Strong shock boundary layer interactions at the leading edge will produce larger shock angles than predicted by inviscid theory, resulting in higher electron concentrations. Also, since the beryllium heat sink nose cap was ejected at about 56 km (near its melting point), teflon ablation products in the flowfield increase the electron concentration over the theories presented here. Finally, since the vehicle was only 1.3 m long with a 0.3 m nose diameter and the total wind angle was oscillating between 2° and 6° (both pitch and yaw wobble) the flowfield was unsteady and wake flow likely contributed to signal attenuation. Since the effects of ambipolar diffusion are not included, errors are expected[17] in the computed electron concentration above 70 km. The RAM C-II vehicle transmitted at a frequency $f = 259.7$ MHz.

The effective attenuation coefficient for the RAM C-II vehicle varied from about 30° at the onset of blackout, dropped below 20° for a short while, and was about 22° at the end of blackout. Overall, the RAM C-II vehicle behaved much more like a simple slender body, accounting for the errors as mentioned above, than the shuttle orbiter. It should be noted that errors are expected when using a two-dimensional wedge approximation for an axisymmetric configuration. Conical flow solutions would result in larger cone angles (than wedge angles) for a similar attenuation coefficient.

Air-Breathing Hypersonic Flight Testing

With a little bit of insight into the complications of blackout prediction at various points in a trajectory, as well as configurational effects, an investigation into the blackout phenomena for air-breathing configurations can be done. Figure 14 shows the calculated values for plasma frequency as a function of trajectory position for four different wedge angles. The range of plasma frequencies of interest on the figures are ω_p = 1E9 s^{-1} to 1E11 s^{-1} which translate to transmissions frequencies of f = 0.16 GHz to 16.0 GHz. The air-breathing flight corridor has been overlaid for reference. Air-breathing hypersonic vehicle configurations will be significantly different than either of the two extremes presented above, but sources of error will be similar, such as shock boundary layer interaction effects (making slender bodies appear much blunter), frozen flow, and ambipolar diffusion. As expected the trends show that the more slender the body, the higher the altitudes and Mach numbers are before blackout occurs for frequencies in the S, C, X, and Ku-bands.
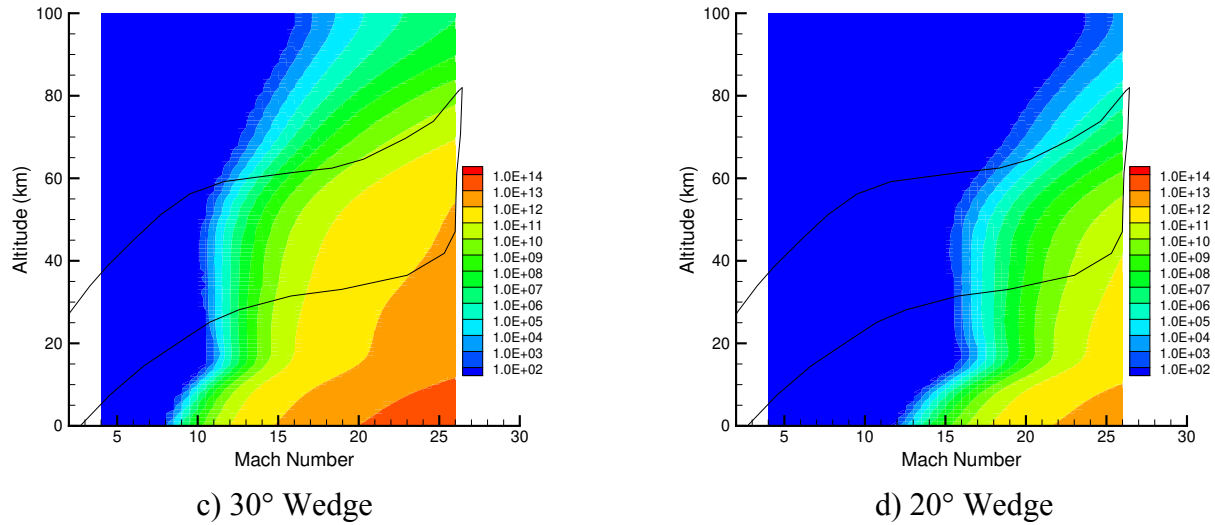

a) 90° Wedge   b) 40° Wedge
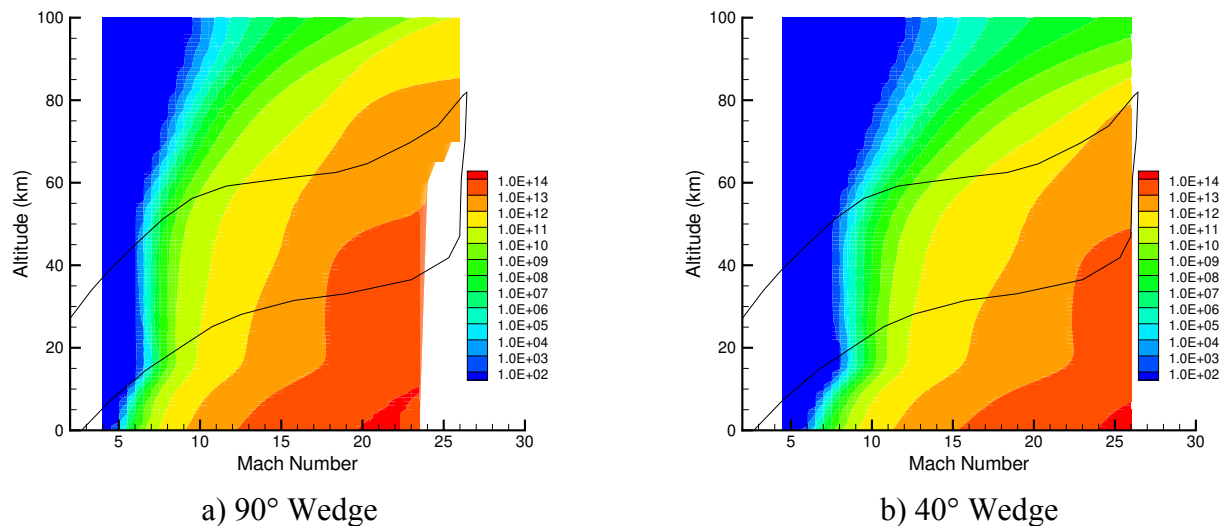
Figure 14: Plots of Mach number versus altitude with plasma frequency contours for four different wedge angles. Solid lines indicate the air-breathing flight corridor.

Applied Normal Magnetic Field

A magnetic field is applied normal to the plasma interface with flux densities of 0, 1, and 5 Tesla. Incident electromagnetic telemetry waves at 2.45 GHz, 10 GHz, and 20 GHz are interacted with the magnetoactive plasma field over the range of Mach numbers and altitudes used in the hypersonic, air-breathing flight corridor. Plots for a normal shock, 40 degree wedge, and 30 degree wedge are shown in Figs.15 and 16 for RHCP waves and for LHCP waves, respectively. Plots for a 20 degree wedge were not shown since the contours were mostly off of the axis shown. Also, Fig. 15c only shows contours for $\mathbf{B}_0$ = 0 T since the others fell outside the limits of the plot. As before, each contour is the attenuation constant unity line (α_p = 1 m^{-1}) where the right side of each line indicates total blackout and the left side of each contour is essentially unattenuated transmission. The first three contours on the left hand side are for $\mathbf{B}_0$ = 0 T, the second three for $\mathbf{B}_0$ = 1 T, and the three

contour on the right are for $\mathbf{B}_0$ = 5 T. For each plot the solid line is for f=2.45 GHz transmission, the dashed line for f=10 GHz transmission, and the dash-dot-dot line for f=20 GHz transmission.
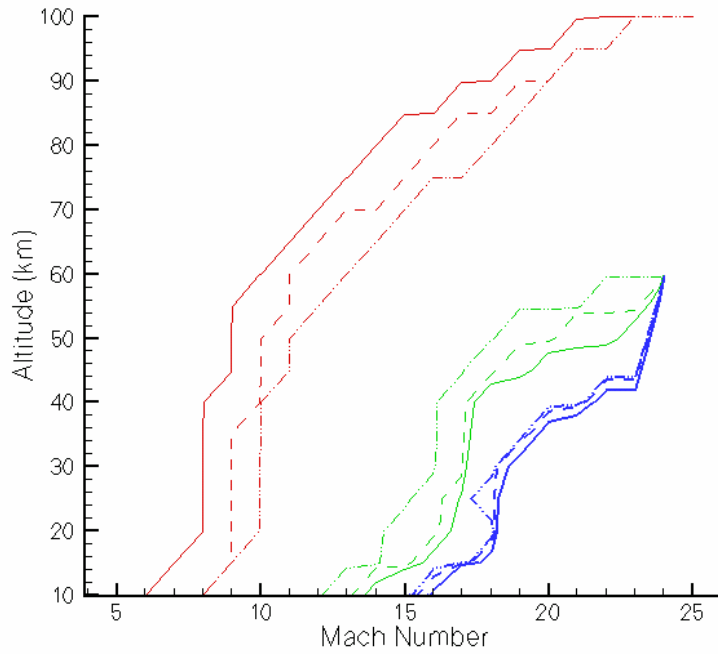
a) 90 degree wedge.
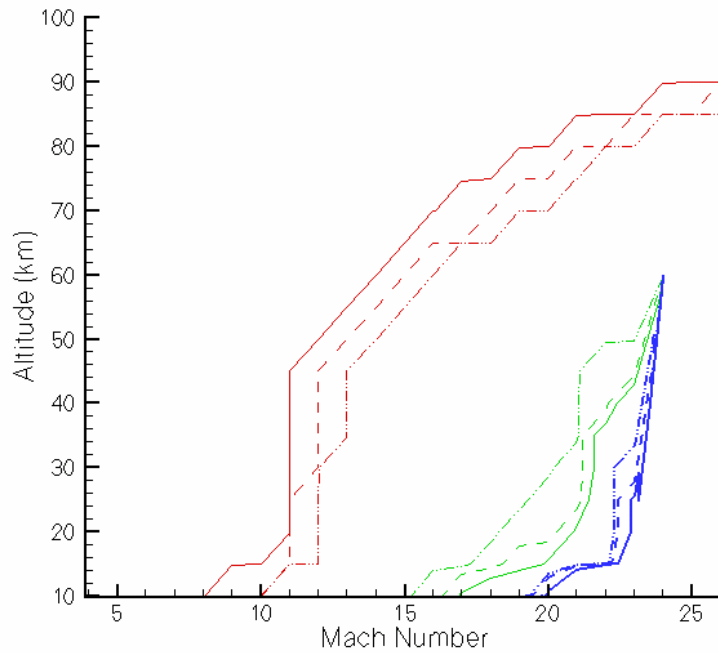
b) 40 degree wedge.
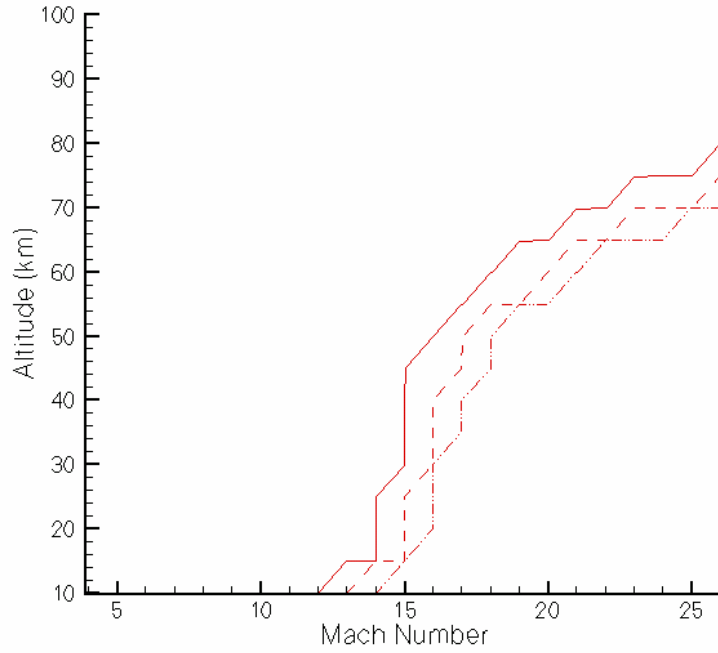
c) 30 degree wedge.

Figure 15: Mach number versus altitude with plasma attenuation constant unity lines for contours of f$_{RHCP}$ = 2.45, 10, 20 GHz and B$_0$ = 0, 1, 5 T.

a) 90 degree wedge.

b) 40 degree wedge.
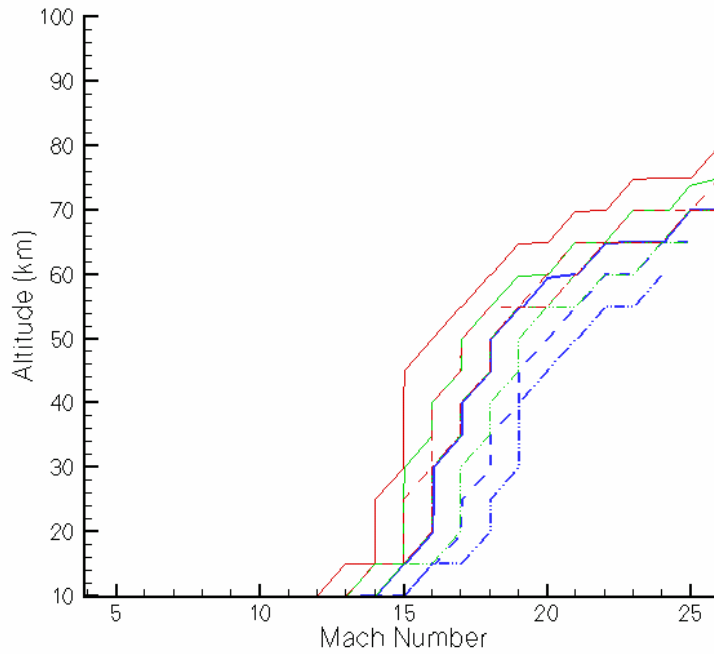
c) 30 degree wedge.

Figure 16: Mach number versus altitude with plasma attenuation constant unity lines for contours of fL_{HCP} = 2.45, 10, 20 GHz and B_0 = 0, 1, 5 T.

The RHCP waves show that an increased in transmission frequency moves the cutoff point to higher Mach numbers and higher altitudes. However, much more benefit can be seen by using a magnetic field flux density of 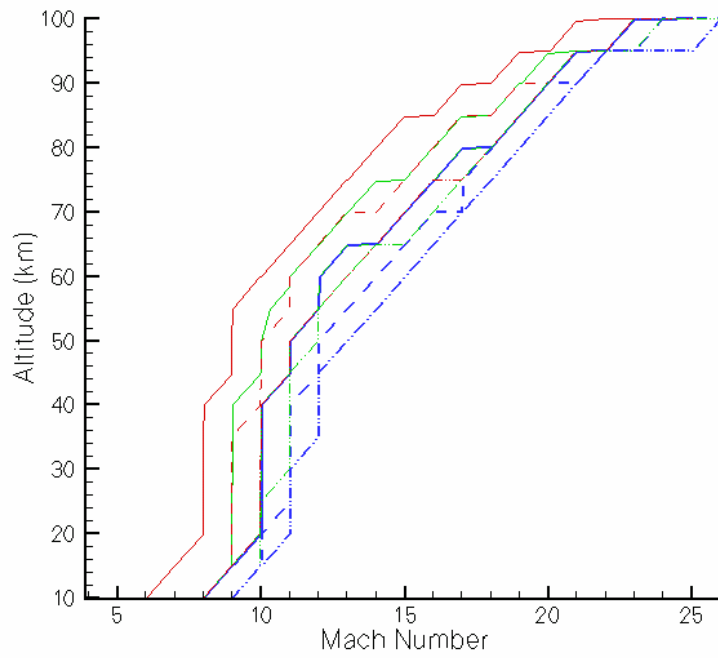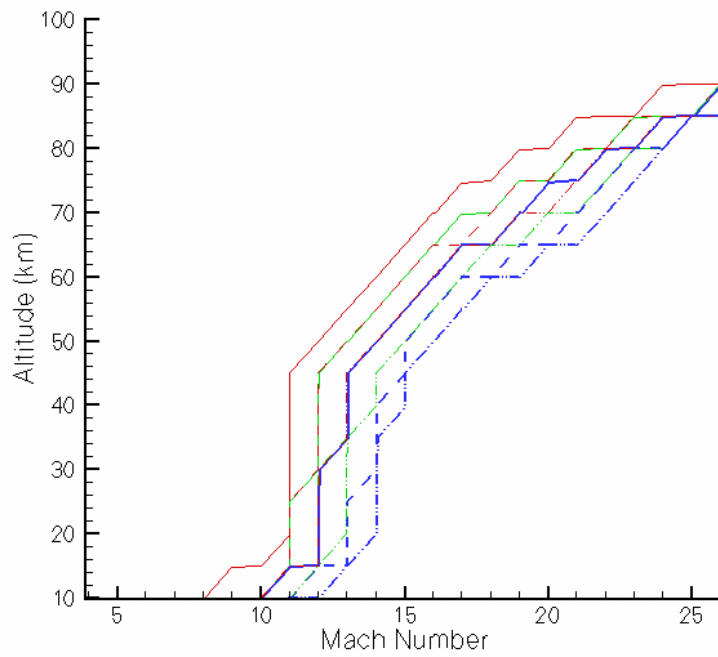just 1 Tesla. The benefits of going from a 1 Tesla to a 5 Tesla magnetic field flux density were not as pronounced. As expected, the LHCP waves perform quite poorly, although some benefits can be seen by both increased transmission frequency and increased magnetic field flux densities.

As was noted above, the contours shown here are only for a single point analysis at the interface of the plasma and only for α_p = 1 m^{-1}. More work is required to couple the effects of the magnetic field to a vehicle generated plasma. The thicker the plasma sheath is the stronger the magnet will be to be to penetrate it.

The exercise of approximating a complex configuration along a three-dimensional trajectory with an unsteady flowfield using a single point shock comparison calculated using an inviscid, steady, nonequilibrium plasma chemistry approach has been detailed. Comparisons to flight data for both the space shuttle orbiter and RAM C-II re-entries have been done to understand the nature of the approximations. The approximation was then applied to the air-breathing hypersonic vehicle flight regime resulting in approximate bounds for blackout frequencies for simple body approximations.

The telemetry blackout caused by the re-entry plasma sheath is still of concern today. With this in mind, a simple framework for analyzing the effects of the interaction of an electromagnetic wave with a magnetoactive plasma layer has been utilized. With the benefits of aerodynamic shaping promised through new high temperature materials, the ability to tailor the flowfield to minimize electromagnetic attenuation is possible. Also, as magnet technology advances, the use of stronger magnetic fields with reduced weight, power, and volume penalties are available. By coupling these technologies, vehicles may be designed to minimize or eliminate telemetry blackout.

Current work is focusing on increased understanding of the interaction between an electromagnetic wave and magnetoactive plasma layer for telemetry applications and applying the methodology to more representative plasma layers. Also, integrated effects through the plasma sheath are being pursued.

VI. HISTORICAL REVIEW OF REENTRY FLIGHT EXPERIMENTS

Work in the first year has uncovered a substantial number of relevant studies for shock-layer telemetry. Some of these are detailed below:

1. USA's RAM Program

The RAM program consisted of eight experimental flights spanning 1961 to 1970[11] coupled with theoretical analysis[27] and ground testing.[28] All of the communication blackout alleviation techniques described above were tested during the RAM program although quantitative details were only reported in the classified literature. However, the program was successful (other than one rocket failure) in providing ample detail into the reentry plasma environment and many tests of different alleviation techniques. All of the tests were performed using a simple conical vehicle configuration,[29] as shown in Figure 17. By using three different scale vehicles, and reentry velocities of either 5.5 km/s or 7.5 km/s, the effects of scaling on the plasma sheath and electron concentrations were also determined. Tests included the use of both water and electrophilic injection through a variety of ports placed in different configuration on the vehicle body. The nozzle schematics are also shown in Figure 17. The water addition was shown to somewhat alleviate the blackout communications problem, but not to the degree expected. Although the exact degree was not openly published, details of the injectors were published.[11, 27, 28, 29]

2. USA's Mercury and Gemini Program's

The flights of both the Mercury 6 and Gemini 3 vehicles resulted in a large amount of information being collected on the plasma sheath properties based on signal strengths received at various ground stations. In these instances, the theoretical pure air models used predicted electron
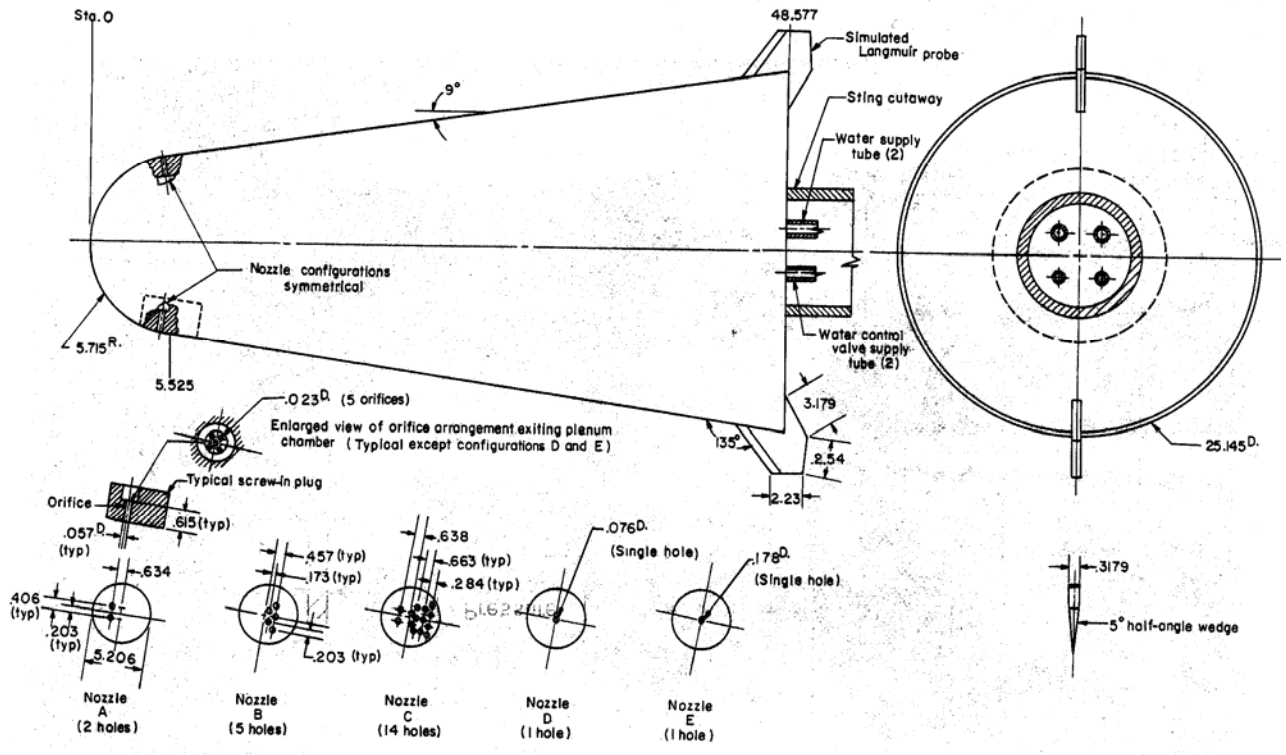
Figure 4.- Schematic of model and nozzle configurations. All dimensions are in centimeters unless indicated otherwise.

Figure 17: Ram-C vehicle design with various nozzle configurations.

densities about 100 times lower than were recorded. The conclusion was that the signal attenuation was not due to pure air plasma at lower altitudes; rather, it was attributed to the presence of ionized heat shield ablation products in the flowfield. A pictorial example[30] of the flowfield around the Gemini 3 spacecraft with the associated antenna locations is shown in Figure 18.

Both the Mercury 6 and Gemini 3 flights involved tests for alleviation of plasma sheath communication attenuation using water injection. The qualitative results of the Gemini 3 flight were that radio frequencies were successfully transmitted through a window in the sheath created by the water spray. The water spray was responsible for large decreases in the temperature and electron density inside the separated flow region, as shown in Figure 18.

Figure 18: Gemini reentry vehicle flowfield.

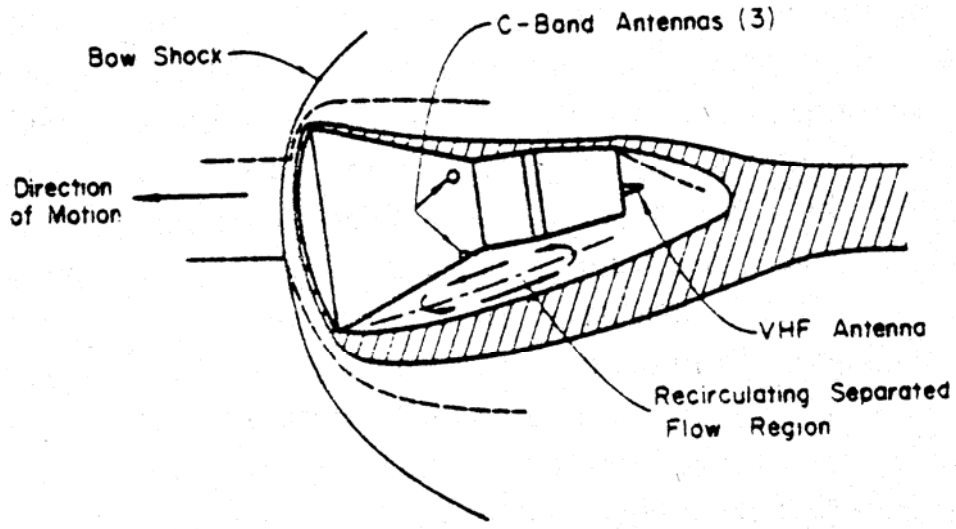### 3. USA's Trailblazer Program

The Trailblazer-II program was carried out by the United States Air Force in conjunction with Ohio State University.[1,17,18,19,20,27,28,29,30,31] An example pictorial of the Trailblazer-II vehicle during its 5.5 km/s reentry is shown in Figure 19.

This program contributed much to the understanding of plasma physics and alleviation techniques. Most notably were the conclusions that the importance of angle of attack and antenna location cannot be overemphasized. This was evident during one portion of the reentry, where there were minimal plasma effects while the ring antenna was on the leeward side of the cone, but was in a blackout condition while on the windward side. This drastic difference in the plasma attenuation characteristics was due solely to the change between a +10 degrees and a −10 degrees angle of attack.

A subsequent flight using an aerodynamic gas spike on the Trailblazer vehicle did not produce qualitative results on the alleviation of plasma blackout since it was activated at an altitude too low to be effective. However, the study did give conservative estimates that the angle of attack
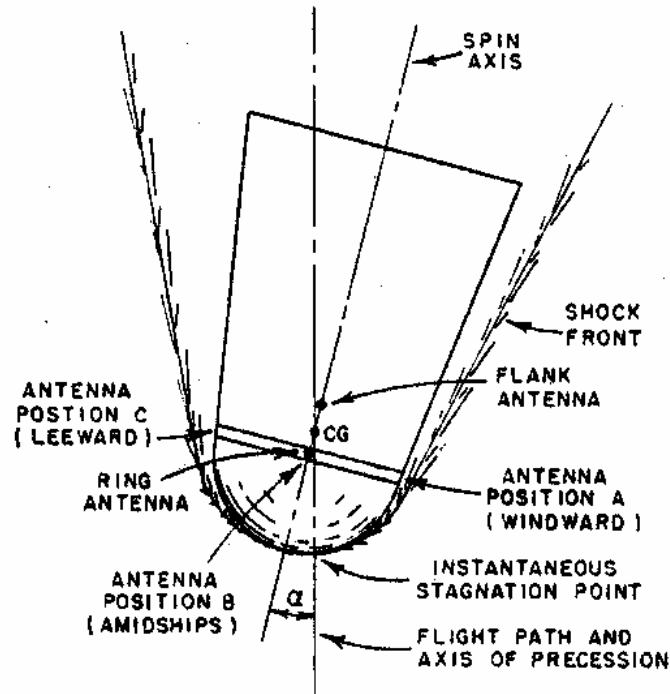
Figure 19: Trailblazer reentry vehicle flowfield.

on the spike must be lower than 5 degrees to be effective. In reality, indications were that the angle of attack must be even lower.

4. Russia's Bor/Buran Program

One of the most recently published works on a reentry flight vehicle designed with alleviation of the communication blackout problem was by Belov et al. for the Russian Bor and Buran vehicles. This work involved the addition of a large remote antenna assembly (RAA) to the front of the reentry vehicle, as shown in Figure 20. The proposed RAA sticks out in front of the vehicle bow shock and must be aligned very closely to the flightpath angle during reentry for successful transmission (as was concluded by the aerodynamic gas spike test of the Trailblazer-II program). Even though the RAA is outside the realm of the vehicle bow shock, it is still encased in
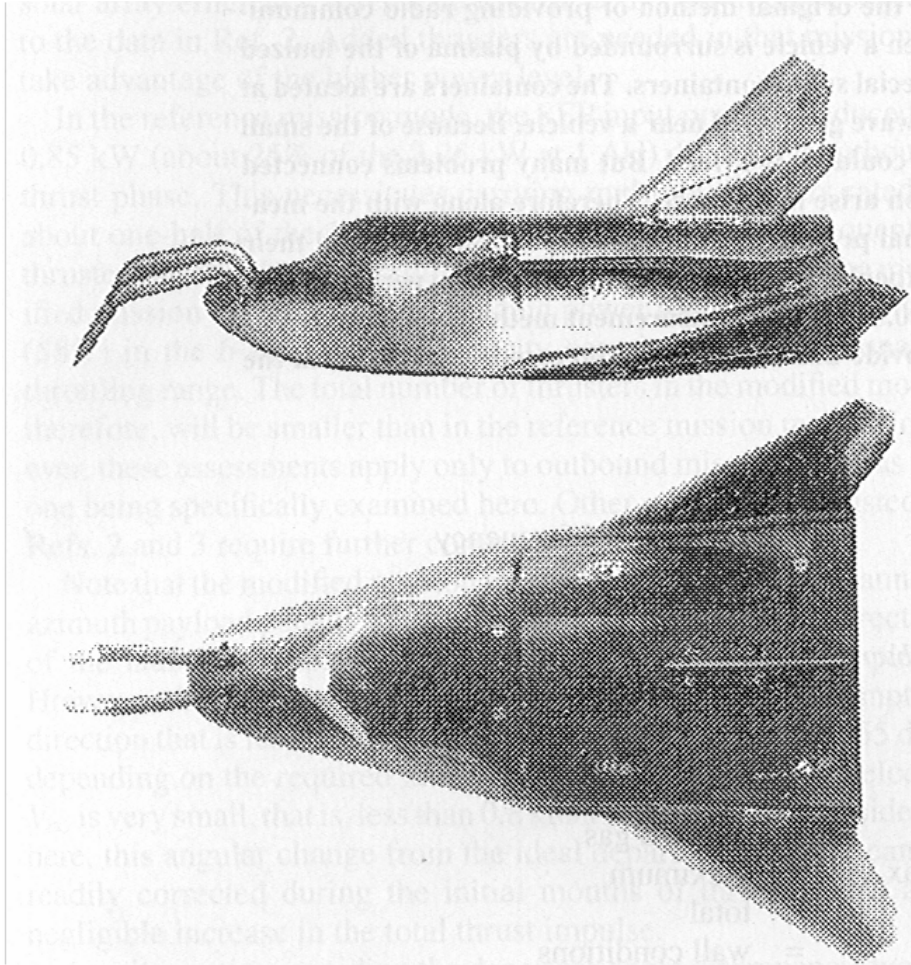
Figure 20: Bor vehicle model with the remote antenna assembly.

its own shock. By being a fairly slender body which is aligned to the reentry flightpath, the RAA

shock is much weaker and therefore the ionization is less severe and concentrated to a thinner layer.

Of course, with any external modification to the flight vehicle as this, there are associated penalties

in C_L, C_D, and most notably in C_m.

Although success was claimed for this project for the ability to communicate through the

plasma sheath (experimentally), many additional problems were created by the flowfield

interactions between different components of the RAA and also between the RAA and the vehicle.

Of particular concern were the shock interactions with the vehicle surface, which required the use

of ablative material for both the antenna and the front of the vehicle. Also, in order to reduce heating rates and the ionization level at the leading edge of the probe, air was ejected through the porous nose cone. Airflow rates greater than 0.7 g/s were required to reduce the surface temperature to under the requirement of 1,000 K. The electromagnetic wave transmissions for this project were in the 0.1 to 0.01 m wavelengths. This solution provides insight into the hypersonic reentry flowfield, slender body plasma characteristics, and antenna interactions, but the addition of the large external antenna is not deemed as a satisfactory answer to the communication blackout problem; many problems were introduced to solve one.

Overall, the most promising techniques for eliminating the reentry communications blackout phenomena will likely be a combination of techniques. The use of a magnetic window or electrophilic injection coupled with high frequency transmission looks to be a favorable solution.

VI. NUMERICAL SOLUTIONS

This project will examine several techniques for plasma telemetry that depend on the use of sharp leading edges to concentrate ionization near a leading edge, thus permitting telemetry farther downstream. To this end, work in the first period concentrated on the class of power-law leading edges that includes a broad spectrum of sharp-to-blunt geometries. The selected approach is to compute the flowfield structure, aerodynamic surface quantities and shock wave structure over these shapes by using the Direct Simulation Monte Carlo[32] (DSMC) method assuming rarefied hypersonic two-dimensional flow. A neutral flow code was developed and implemented in this first year, with temperature contours being used to estimate degree of ionization.

In the second period, work has concentrated on the continuation and validation of the DSMC code to handle the different types of reactions leading to ionization, as well as recombination. Charged particles and their associated fields are being added to the simulations in order to capture ionization effects (i.e., predict electron concentrations) and their effect on radio wave attenuation.

In order to assess the overall performance of the power law shaped leading edges, a parametric study related to the effect of freestream Mach number, freestream Knudsen number, wall temperature, angle of attack and gas-surface interactions was explored. The application of DSMC has been aimed primarily at the transition regime that is characterized by Knudsen numbers that are above the upper limit for the validity of the Navier-Stokes equations but below the level at which the flow falls into the collisionless flow of the free molecular regime. In the transitional flow regime, both drag and aerodynamic heating are very sensitive to the degree of rarefaction. It is important to emphasize that, in this first two periods, results are for uncharged fluid, and thus only

form the basis for later ionization results. The final reporting period will include the introduction of charged particles in the DSMC solution.

Two fundamental quantities for gas dynamic flow are velocity and number density. These quantities are neither inferred nor dependent on the condition of thermal equilibrium, such as the case for pressure and temperature. The differences in the descriptions of equilibrium and nonequilibrium flows result from differences in the thermodynamic behavior of the gas, the dynamic aspects being the same. Hence, attention will be paid first to velocity and density properties followed by temperature and pressure properties.

Normal velocity profiles along the stagnation streamline and their dependence on the power law exponent are illustrated in Figure 21. Shown in this figure is also the normal velocity profile for the circular cylinder case. Each profile has been taken through cell centroids that lie very close to the stagnation line, and therefore can be considered as being along the stagnation streamline. $\eta \lambda_\infty$ is the dimensionless distance away from the body. In Figure 21, the normal velocity v is expressed as a fraction of the freestream velocity U_∞. As can be seen, these profiles show a gradual merging of the shock layer and shock wave with decreasing the power law exponent n. As n increases, the velocity profile becomes steeper indicating that the shock structure becomes thinner. For instance, the velocity reduction in a distance of one freestream mean free path upstream the leading edge is around 90% for the circular cylinder, 60% for the $n = 1/2$ case and only 10 % for the $n = 0.8$ case. As a point of reference, the Rankine-Hugoniot relations give a post shock velocity ratio (normalized by the freestream velocity) of 17%.

In simulating rarefied flows, the computational flow domain must extent far enough upstream of the body to provide ample opportunity for freestream molecules to interact with those molecules that have reflected from the body and are diffusing into the flow. Insufficient upstream
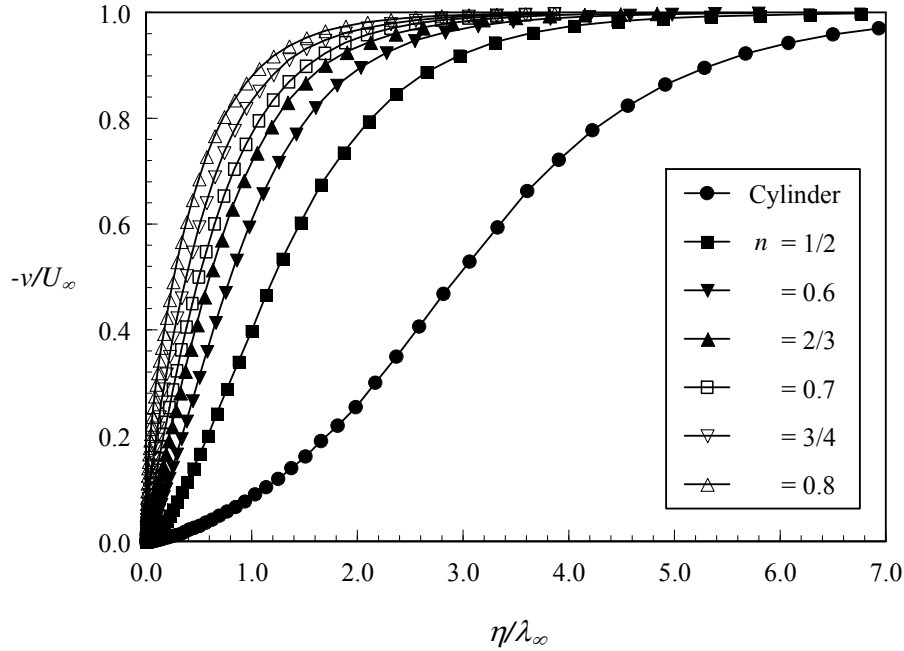
Figure 21: Dimensionless normal velocity ($-v/U_\infty$) profiles along the stagnation streamline for the circular cylinder and various power law leading edges.

domain size leads to overprediction of aerodynamic heating and forces. Figure 21 demonstrates that the shape of the leading edge influences the flowfield far upstream. This domain of influence increases with decreasing the power law exponent. This influence is still stronger for the circular cylinder, since it is blunter than the power law leading edges. This results from upstream diffusion of particles that are reflected from the nose of the leading edge. Therefore, blunting the nose of the leading edge (decreasing n, or increasing the curvature radius R_c) leads to significantly larger disturbance upstream of the body.

Figure 22 presents the velocity slip u_w, normalized by the freestream velocity U_∞, along the body surface as a function of the body slope angle θ. It is seen that velocity slip increases from zero at the stagnation point up to a maximum value at station $\theta \approx 20°$ for the power law leading edges. For the $n = 1/2$ case the flow expands slowly, and the maximum velocity slip is 6% of the
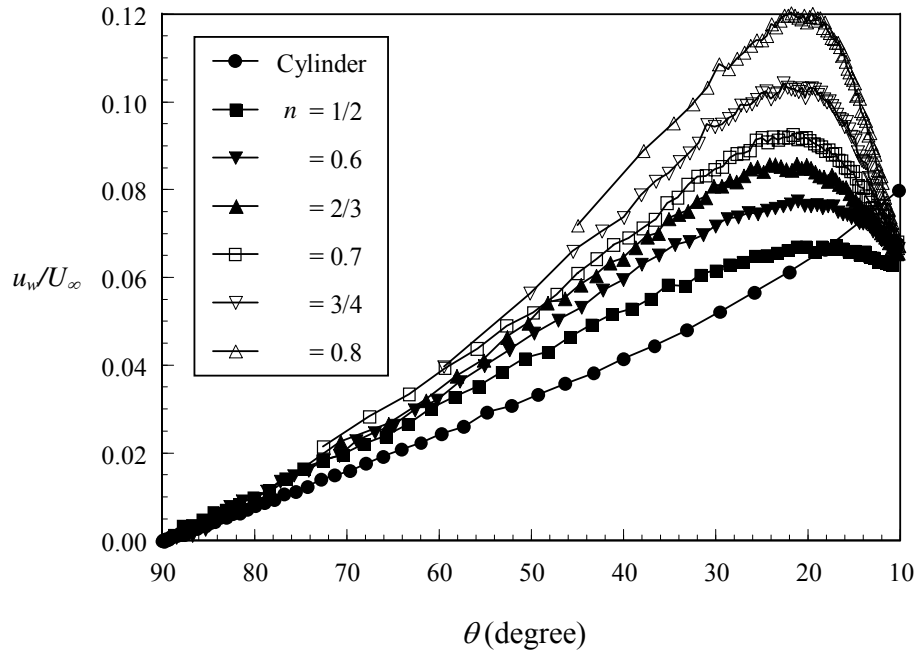
Figure 22: Dimensionless velocity slip (u_w/U_∞) profiles along the body surface for the circular cylinder and various power law leading edges.

freestream velocity. For the $n = 0.8$ case, the maximum velocity slip is 12 % of the freestream velocity. Hence, it means that the outer extent of the flowfield disturbance above the surface is much smaller for the leading edge shape with power law exponent of 0.8 than that for 1/2. It is interesting to note that as the power law exponent increases the position of the maximum value is displaced closer to the stagnation point. As a reference, in terms of arc length along the body, the station $\theta \approx 20°$ corresponds to $s/\lambda_\infty \approx 5.0$ and 0.7 (see Figure 3.4) for power law exponents of 1/2 and 0.8, respectively. Therefore, for power law exponent of 0.8 the maximum velocity slip is double that for the $n = 1/2$ case and takes place one order of magnitude closer to the stagnation point, as compared to $n = 1/2$ case.

The outer extent of the flowfield disturbance above the surface is better seen in Figure 23. This figure presents a set of profiles for the tangential velocity u plotted versus height η and

parameterized by the surface slope angle θ along the body. In an effort to emphasize points of interest, the tangential velocity profiles are shown for six stations along the body represented by the surface slope angles of 70, 60, 50, 40, 30 and 20 degrees. The tangential velocity u_∞, defined as $\eta \rightarrow \infty$, is also shown for each station, normalized by U_∞. Because of the body curvature, u_∞/U_∞ varies as a function of the body slope. Interesting features can be drawn from these sets of tangential velocity profiles. As the body slope decreases the tangential velocity adjacent to the body surface increases. This is to be expected since the flow experiences an expansion as it moves downstream. Major differences are observed in the tangential velocity due to changes in the power law exponents.

It is seen that the flow accelerates faster as the power law exponent increases. By increasing the power law exponent, the radius of curvature of the nose decreases, and the flow behavior in the vicinity of the nose of the leading edges changes aerodynamically from blunt to sharp one. As a result, the tangential velocity increases since the nose geometry minimizes disturbances in the flowfield. Also, it is seen that the tangential velocity profiles for the power law cases spread out when compared with that for the circular cylinder case, indicating the flow expansion along the body surface is much slower for the circular cylinder than that for the power law cases.

For the circular cylinder, there is an inflection point in the tangential velocity profiles for stations $\theta \le 50°$, which becomes more pronounced as the flow expands downstream along the body surface. This inflection point, which is associated with a pressure increase (see next sections), is not observed in the velocity profiles for the power law cases. Also for the circular cylinder case, there are substantial velocity gradients all the way across the shock layer.
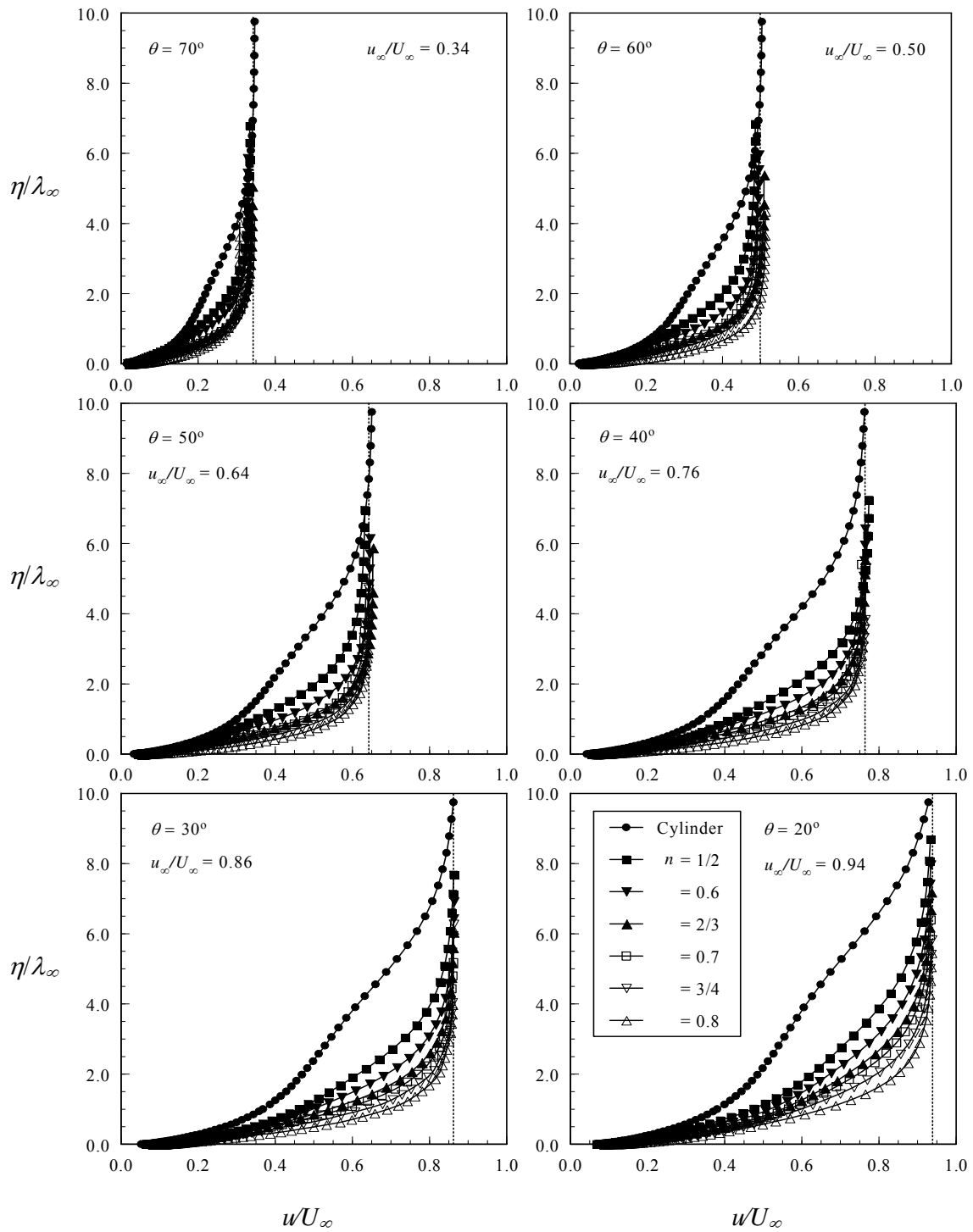
Figure 23: Dimensionless tangential velocity (u/U_∞) profiles along the body surface for the circular cylinder and various power law leading edges.

61

Another interesting characteristic in these plots is the similarity of the velocity profiles along the body surface. This is an indication that the velocity profiles may be expressed in terms of functions that, in appropriate coordinates, may be independent of one of the coordinate directions. However, no attempts have been done to find such functions.

To demonstrate the current capability, finalized in the first reporting period, kinetic temperature profiles along the stagnation streamline, normalized by the freestream temperature T_∞, are plotted in **Error! Reference source not found.** and **Error! Reference source not found.** for the circular cylinder. **Error! Reference source not found.** emphasizes the upstream propagation of the temperature disturbances, while **Error! Reference source not found.** emphasizes the region close to the stagnation point. Shown in Figure 26 are the kinetic temperature profiles for the power law shaped leading edges investigated. From both sets of Figures, it can be seen that the temperature profiles for the power law leading edges follow the same trend as those presented by the circular cylinder.

Thermodynamic nonequilibrium is also observed throughout the shock layer, as shown by the lack of equilibrium of the translational and internal kinetic temperatures. Thermal nonequilibrium occurs when the temperatures associated with the translational, rotational, and vibrational modes of a polyatomic gas are different. The overall kinetic temperature T_{ov} shown is defined for a nonequilibrium gas as the weighted mean of the translational and internal temperatures as being,

$$T_{ov} = \frac{\zeta_t T_t + \zeta_r T_r + \zeta_v T_v}{\zeta_t + \zeta_r + \zeta_v} \qquad (11)$$

where ζ stands for the degree of freedom.

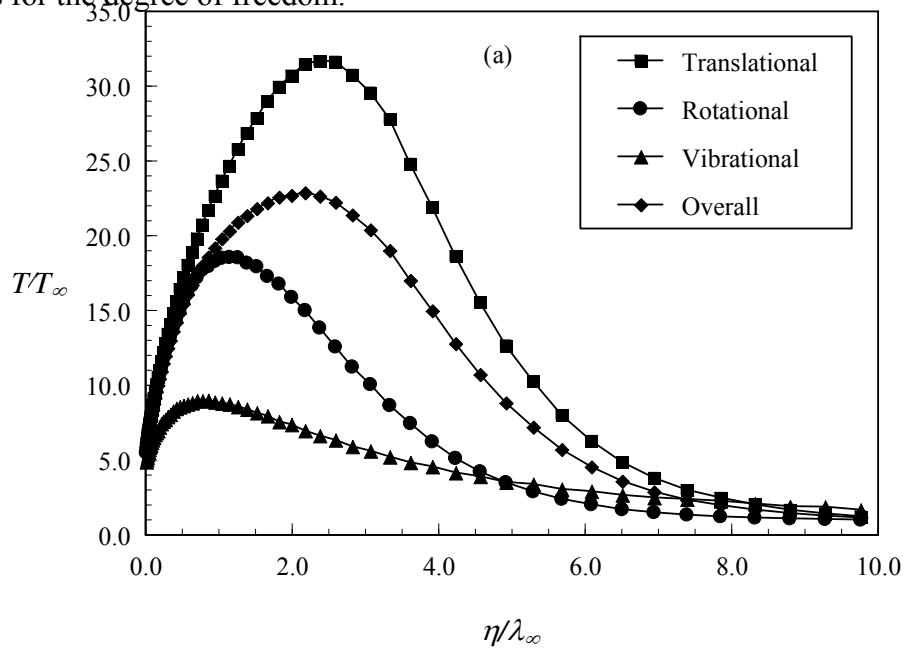**Figure 24: Dimensionless kinetic temperature (T/T_∞) profiles along the stagnation streamline for the circular cylinder.**
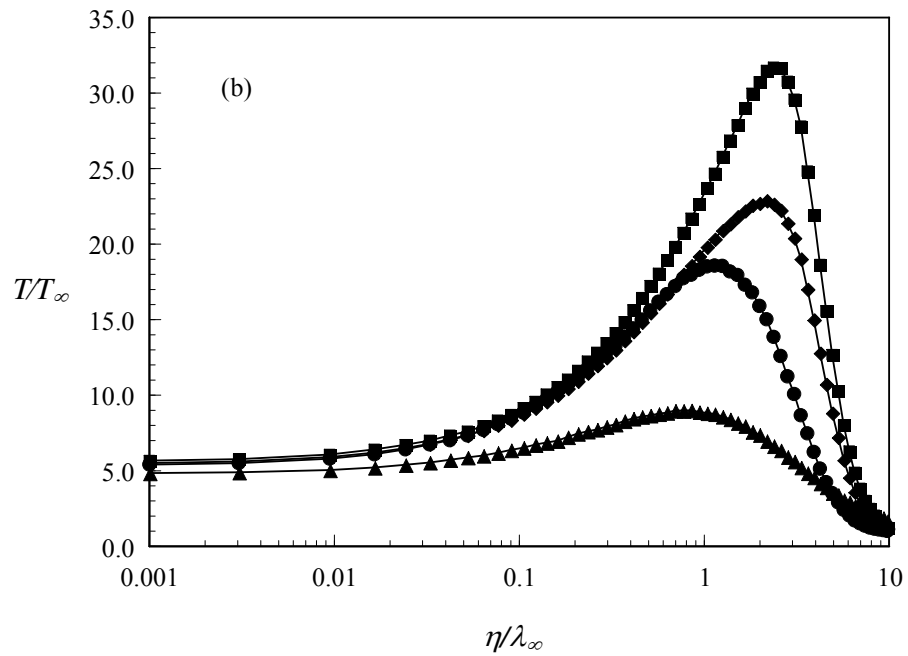

Figure 25: Dimensionless kinetic temperature (T/T_∞) profiles in the vicinity of the stagnation point for the circular cylinder.
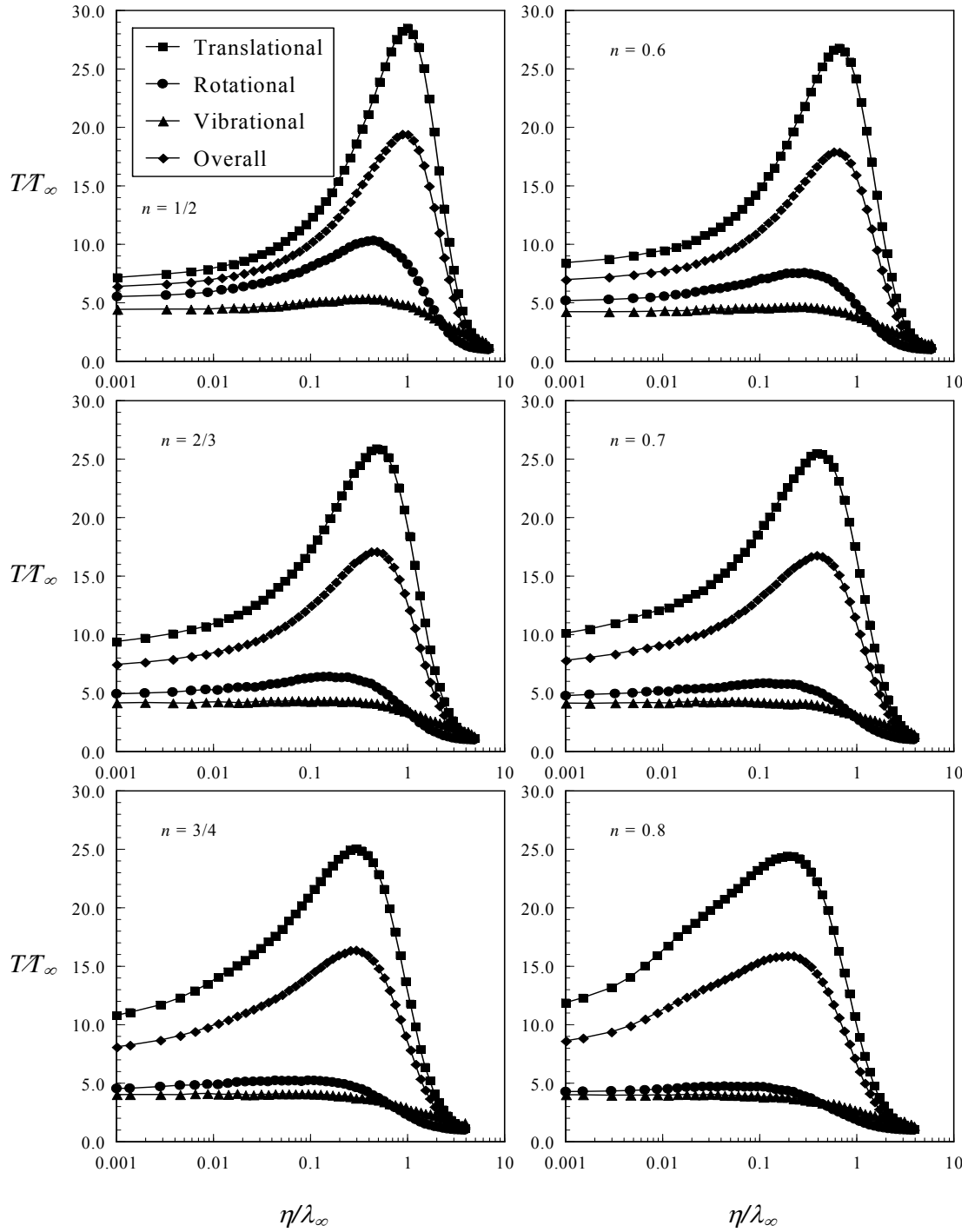
Figure 26: Dimensionless kinetic temperature (T/T_∞) profiles along the stagnation streamline for various power law exponents.

It is important to observe that the ideal gas equation of state does not apply to this temperature in a nonequilibrium situation. The overall kinetic temperature is equivalent to the thermodynamic temperature only under thermal equilibrium conditions.

According to Figure 26, in the undisturbed freestream far from the body, the translational and internal kinetic temperatures have the same value and are equal to the thermodynamic temperature. Approaching the nose of the body, the translational kinetic temperature rises to well above the rotational and vibrational temperatures and reaches a maximum value that is a function of the power law exponent. Since a large number of collisions are needed to excite molecules vibrationally from the ground state to the upper state, the vibrational temperature increases much more slowly than rotational temperature. Still further upstream toward the nose of the body, the translational kinetic temperature decreases and reaches a constant value on the wall that is above the wall temperature, resulting in a temperature jump as defined in continuum formulation. The temperature jump increases as the power law exponent increases.

The temperature distribution above the body surface is shown more clearly in Figure 27. This Figure displays a set of the translational kinetic temperature profiles plotted versus dimensionless height η/λ_∞ and parameterized by the surface slope angle θ along the body. The translational kinetic temperature profiles present basically the same trend above the body as the flow experiences an expansion. However, specific details may appear. The circular cylinder and power law shapes defined by $n < 3/4$ present no significant variations in the translational kinetic temperature adjacent to the wall, along the body surface. The comparison of the temperature profiles for the $n = 0.8$ case against those for the other cases shown in Figure 27 indicates that the translational kinetic temperature for the $n = 0.8$ case is still decreasing in the range $0 \leq \eta/\lambda_\infty <$ 0.001, for stations in the range from 70° to 50°. Similarly to density, great variations arise in the
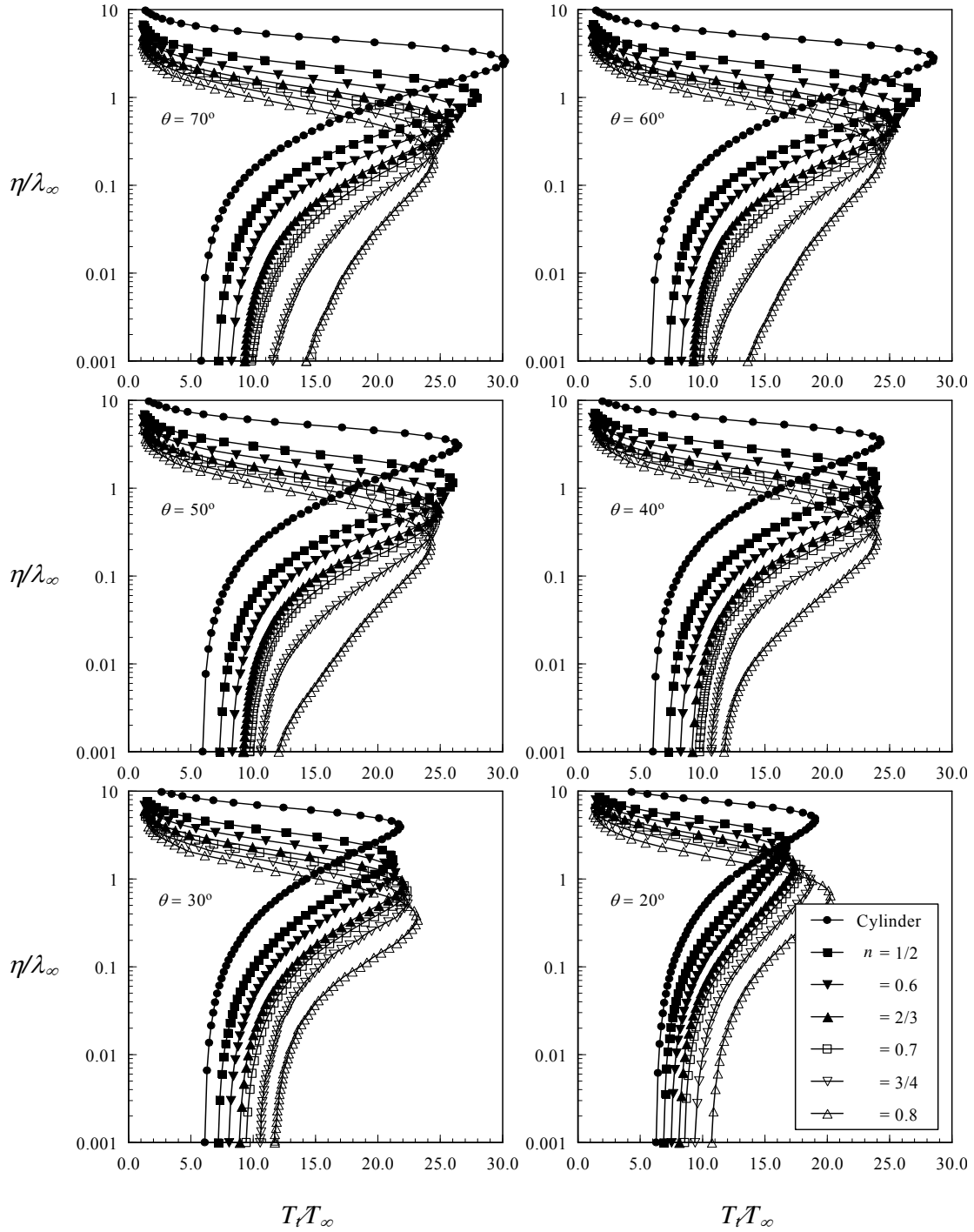
65

Figure 27: Dimensionless translational kinetic temperature (T_t/T_∞) profiles along the body surface for the circular cylinder and various power law leading edges.

translational temperature ratio in this thin layer where the temperature ratio changes approximately

from 15 to 11 (not shown).

66

CONCLUSIONS

From the time that man started venturing into the realms of space, the problems associated with communication blackout due to the plasma sheath have been studied analytically, experimentally, and with flight test vehicles. Unfortunately, little progress has been made in the last 40 years towards solving this problem in a robust and acceptable manner, although small strides have been made. Due to security concerns, much of the information on the progress that has been made in these areas remains classified.

Through the result of many years of research, accomplishing the milestone of building and flying an air-breathing hypersonic cruise vehicle seems to be looming just over the horizon. Extending the yet unfinished work of achieving telemetry through plasma layers from the reentry environment to the sustained hypersonic cruising environment is now required more imminently then ever. The need to eliminate the communication blackout problem is critical for T&E of hypersonic cruise and access to space vehicles, which will spend a considerable amount of time in earth's atmosphere, likely enveloped in a plasma sheath. Since the plasma environment is highly dependent on the vehicle configuration, flight path angle, and flight velocity, the proper design of an air-breathing hypersonic vehicle will need to incorporate the T&E telemetry concerns into the base level design requirements. Including T&E concerns after the fact for air-breathing hypersonic vehicles would most likely make testing impossible or required substantial redesign of the vehicle. Any post production vehicle enhancements made to satisfy T&E telemetry requirements would likely be very costly, time consuming, and most importantly, disrupt the small vehicle performance margins.

The most promising techniques for eliminating the reentry communications blackout phenomena will likely be a combination of techniques. Aerodynamic shaping of the vehicle, especially the leading edge, will play a major role in tailoring the flowfield properties to make telemetry through the plasma sheath of a hypersonic cruise vehicle possible. Coupled with this, methods of active flowfield modification using electrophilic injection or imposing a magnetic field, will benefit from the reduced electron concentrations achievable through aerodynamic shaping.

LIST OF PUBLICATIONS

1. Santos, W., and Lewis, M. J., "Power Law Shaped Leading Edges in Rarefied Hypersonic Flow", presented at the 40th AIAA Aerospace Sciences Meeting and Exhibit, Reno, NV, January 14-17, 2002.

2. Starkey, R. P., Lewis, M. J., and Jones, C. H., "Active Flowfield Modification for Plasma Telemetry", presented at the 6th Annual International Test and Evaluation Association Instrumentation Conference, Lancaster, CA, April 30, 2002.

3. Starkey, R. P., and Lewis, M. J., "Aerodynamic Shaping Effects on Reentry Plasma Sheath Telemetry Blackout", presented at the AIAA/AAAF 11th International Space Planes and Hypersonic Systems and Technologies Conference, Orleans, France, Sept 29-Oct 4, 2002.

4. Starkey, R. P., Lewis, M. J., and Jones, C. H., "Plasma Telemetry in Hypersonic Flight", presented at the 2002 International Telemetering Conference, San Diego, CA, October 21-24, 2002.

5. Santos, W., and Lewis, M. J., "Shock Wave Structure in a Rarefied Hypersonic Flow on Power Law Shaped Leading Edges", presented at the 41st AIAA Aerospace Sciences Meeting and Exhibit, Reno, NV, January 6-9, 2003.

6. Starkey, R. P., "Electromagnetic Wave/Magnetoactive Plasma Sheath Interaction for Hypersonic Vehicle Telemetry Blackout Analysis", presented at 34th AIAA Plasmadynamics and Lasers Conference, Orlando, FL, June 23-36, 2003.

7. Hoult, D., Starkey, R. P., and Lewis, M. J., "Direct Simulation of Ionization Around Power-Law Leading Edges in Rarefied Hypersonic Flow", presented at 34th AIAA Plasmadynamics and Lasers Conference, Orlando, FL, June 23-36, 2003.

8. Santos, W., and Lewis, M. J., "", presented at 34th AIAA Plasmadynamics and Lasers Conference, Orlando, FL, June 23-36, 2003.

9. Starkey, R., "Nonequilibrium Plasma Effects on Telemetry Effects Considerations for Air-Breathing Hypersonic Vehicle Design", AIAA 2004-0333, presented at the 42nd AIAA Aerospace Sciences Meeting and Exhibit.

REFERENCES

1   Rawhouser, R., "Overview of the AF Avionics Laboratory Reentry Electromagnetics Program," <u>The Entry Plasma Sheath and its Effects on Space Vehicle Electromagnetic Systems, Volume I</u>, NASA SP-252, National Aeronautics and Space Administration, Washington, D.C., 1971, Pages 3-17.

2   Dirsa, E., "The Telemetry and Communication Problem of Re-Entrant Space Vehicles," <u>Proceedings of the Institute for Radio Engineers</u>, Volume 48, April 1960, Pages 703-713.

3   Rybak, J., and Churchill, R., "Progress in Reentry Communications," <u>IEEE Transactions on Aerospace and Electronic Systems</u>, Volume 7, September 1971, Pages 879-894.

4   O'Hare, L., "Maneuvering a Reentry Body via Magneto-Gasdynamic Forces," Ph.D. Dissertation, University of Maryland, College Park, Maryland, 1992.

5   Nusca, M., "Numerical Simulation of Electromagnetic Wave Attenuation in a Nonequilibrium Chemically Reacting Hypervelocity Flow," Ph.D. Dissertation, University of Maryland, College Park, Maryland, 1997.

6   Steinkopf, M., "Mission Accomplished – Final Report on the Atmospheric Reentry Demonstrator," http://esapub.esrin.esa.it/onstation/onstation5/ard5.pdf, March 2001.

7   Starkey, R., Lewis, M., and Jones, C., "Active Flowfield Modification for Plasma Telemetry," Proceedings of the 6th International Test and Evaluation Association Instrumentation Conference, Lancaster, California, April 2002.

8   Starkey, R., "Hypersonic Air-Breathing Missile Designs Within External Box Constraints," Ph.D. Dissertation, University of Maryland, College Park, Maryland, 2000.

9   Brown, A., "Hypersonic Designs With a SHARP Edge," <u>Aerospace America</u>, Volume 35, Number 9, September 1997, Pages 20-21.

10 Kolodziej, P., Bowles, J., Brown, J., Cornelison, C., Lawrence, S., Loomis, M., Merriam, M., Rasky, D., Tam, T., Wercinski, P., Hodapp, A., Deese, D., Pilcher, M., Tucker, R., Bogdanoff, D., Chapman, G., Gage, P., Palmer, G., Venkatapathy, E., Bowling, D., Holt, D., and Yates, L., "SHARP-L1 Technology Demonstrator Development: An Aerothermodynamic Perspective," AIAA Paper 2000-2688, Proceedings of 34th American Institute of Aeronautics and Astronautics Thermophysics Conference, Denver, Colorado, June 2000.

11 Akey, N. D., "Overview of RAM Reentry Measurements Program," in *The Entry Plasma Sheath and its Effects on Space Vehicle Electromagnetic Systems*, Vol. 1, pp. 19-31, NASA Special Publication SP-252, 1970.

12 Huber, P. W., and Sims, T. E., "The Entry-Communications Problem," *Astronautics and Aeronautics*, Vol. 2, Oct 1964, pp. 30-40.

13   Brown, D., and Hendrix, S., "Advanced NASA Communications Satellite Gives Broadband Access New Meaning," NASA News Release 02-40, Mar 2002.

14   Modica, A., Spepakoff, G., and Rosenbaum, H., "A Shock Tube Study of Plasma Alleviation by Oxide Dust," in *The Entry Plasma Sheath and its Effects on Space Vehicle Electromagnetic Systems*, Vol. 1, pp. 531-558, NASA Special Publication SP-252, 1970.

15   Aisenburg, S., and Hu, P. N., "The Removal of Free Electrons in a Thermal Plasma by Means of Rapidly Evaporating Liquid Additives," in *The Entry Plasma Sheath and its Effects on Space Vehicle Electromagnetic Systems*, Vol. 1, pp. 617-622, NASA SP-252, 1970.

16   Parmentier, E. M., Wray, K. L., and Weiss, R. F., "Aerophysical Plasma Alleviation," in *The Entry Plasma Sheath and its Effects on Space Vehicle Electromagnetic Systems*, Vol. 1, pp. 579-616, NASA Special Publication SP-252, 1970.

17   Belov, I. F., Gorelov, V. A., Kireev, A. Y., Korolev, A. S., and Stepanov, E. A., "Investigation of Remote Antenna Assembly for Radio Communication with Reentry Vehicle," *Journal of Spacecraft and Rockets*, Vol. 38, No. 2, Mar-Apr 2001, pp. 249-256.

18   Meyer, B., Nelson, H. F., and Riggins, D. W., "Hypersonic Drag and Heat-Transfer Reduction Using a Forward-Facing Jet," *AIAA Journal of Aircraft*, Vol. 38, July-Aug 2001, pp. 680-686.

19   Hodara, H., "The Use of Magnetic Fields in the Elimination of the Re-Entry Radio Blackout," *Proceedings of the Institute for Radio Engineers*, Vol. 49, Dec 1961, pp. 1825-1830.

20   Rothman, H., Morita, T., and Scharfman, W., "Transmission Through an Ionized Medium in the Presence of a Strong Magnetic Field," in *Electromagnetic Aspects of Hypersonic Flight* (Rotman, W., Moore, H. K., and Papa, R., eds.), pp. 196-212, Spartan Books, Inc., 1964.

21   Mason, W., and Lee, J., "Aerodynamically Blunt and Sharp Bodies," AIAA Journal of Spacecraft and Rockets, Volume 31, Number 3, May-June 1994, Pages 378-382.

22   O'Brien, T., and Lewis, M., "Two-Dimensional Power Law Shapes for Leading Edge Blunting with Minimal Standoff," AIAA Journal of Spacecraft and Rockets, Volume 36, Number 5, September-October 1999, Pages 653-658.

23   Glick, H., "Interaction of Electromagnetic Waves with Plasmas of Hypersonic Flows," American Rocket Society Journal, Volume 32, September 1962, Pages 1359-1364.

24   Evans, J., Schexnader, C., and Huber, P., "Computation of Ionization in Re-Entry Flowfields," AIAA Journal, Volume 8, Number 6, June 1970, Pages 1082-1089.

25   Cambel, A. B., *Plasma Physics and Magnetofluidmechanics*, Mc-Graw Hill Book Company, Inc., New York, 1963.

26   Krall, N. A., and Trivelpiece, A. W., *Principles of Plasma Physics*, Mc-Graw Hill Book Company, Inc., New York, 1973.

27   Dunn, M. G., "Experimental Plasma Studies," *NASA Contractor Report 1958*, 1972.

28   Gooderum, P. G., and Bushnell, D. M., "Atomization, Drop Size, and Penetration for Cross-Stream Water Injection at High-Altitude Reentry Conditions With Application to the RAM C-I and C-III Flights," *NASA Technical Note D-6747*, 1972.

29   Weaver, W. L., and Hinson, W. F., "Water Injection From a 9° Hemisphere-Cone Into a Hypersonic Airstream," *NASA Technical Note D-5739*, 1970.

30   Huber, P. W., "Deduction of Reentry Plasma Properties About Manned Orbital Spacecraft From Radio Signal Attenuation Data," *NASA Technical Note D-4118*, 1967.

31   Caldecott, R., Bohley, P., and Mayhan, J. W., "Radio Frequency Noise During Reentry," *IEEE Transactions on Antennas and Propagation*, Vol. 17, Nov 1969, pp. 786-790.

32   Bird, G. A., *Molecular Gas Dynamics and the Direct Simulation of Gas Flows,* Clarendon Press, Oxford, 1994.